Search for natural and split supersymmetry in proton-proton collisions at $\sqrt{s} = 13$ TeV in final states with jets and missing transverse momentum

The CMS collaboration

E-mail: cms-publication-committee-chair@cern.ch

Abstract: A search for supersymmetry (SUSY) is performed in final states comprising one or more jets and missing transverse momentum using data from proton-proton collisions at a centre-of-mass energy of 13 TeV. The data were recorded with the CMS detector at the CERN LHC in 2016 and correspond to an integrated luminosity of 35.9 fb^{-1}. The number of signal events is found to agree with the expected background yields from standard model processes. The results are interpreted in the context of simplified models of SUSY that assume the production of gluino or squark pairs and their prompt decay to quarks and the lightest neutralino. The masses of bottom, top, and mass-degenerate light-flavour squarks are probed up to 1050, 1000, and 1325 GeV, respectively. The gluino mass is probed up to 1900, 1650, and 1650 GeV when the gluino decays via virtual states of the aforementioned squarks. The strongest mass bounds on the neutralinos from gluino and squark decays are 1150 and 575 GeV, respectively. The search also provides sensitivity to simplified models inspired by split SUSY that involve the production and decay of long-lived gluinos. Values of the proper decay length $c\tau_0$ from 10^{-3} to 10^5 mm are considered, as well as a metastable gluino scenario. Gluino masses up to 1750 and 900 GeV are probed for $c\tau_0 = 1$ mm and for the metastable state, respectively. The sensitivity is moderately dependent on model assumptions for $c\tau_0 \gtrsim 1$ m. The search provides coverage of the $c\tau_0$ parameter space for models involving long-lived gluinos that is complementary to existing techniques at the LHC.

Contents

1 Introduction

Supersymmetry (SUSY) [1–4] is an extension of the standard model (SM) of particle physics that introduces at least one bosonic (fermionic) superpartner for each fermionic (bosonic) SM particle, where the superpartner differs in its spin from its SM counterpart by one half unit. Supersymmetry offers a potential solution to the hierarchy problem [5, 6], predicts unification of the gauge couplings at high energy [7–9], and provides a candidate for dark matter (DM). Under the assumption of R-parity [10] conservation, SUSY particles are expected to be produced in pairs at the CERN LHC and to decay to the stable, lightest SUSY particle (LSP). The LSP is assumed to be the neutralino $\widetilde{\chi}_1^0$, a weakly interacting massive particle and a viable DM candidate [11, 12]. So-called natural SUSY models, which invoke only a minimal fine tuning of the bare Higgs boson mass parameter, require only the gluino, third-generation squarks, and a higgsino-like $\widetilde{\chi}_1^0$ to have masses at or

near the electroweak (EW) scale [13]. The interest in natural models is motivated by the discovery of a low-mass Higgs boson [14–19]. The characteristic signature of natural SUSY production at the LHC is a final state containing an abundance of jets originating from the hadronization of heavy-flavour quarks and significant missing transverse momentum $\vec{p}_{\mathrm{T}}^{\mathrm{miss}}$.

Split supersymmetry [20, 21] does not address the hierarchy problem — in contrast to natural SUSY models — but preserves the appealing aspects of gauge coupling unification and a DM candidate. In such a model, only the fermionic superpartners, and a finely tuned scalar Higgs boson, may be realized at a mass scale that is kinematically accessible at the LHC. All other SUSY particles are assumed to be ultraheavy. Hence, within split SUSY models, the gluino decay is suppressed because of the highly virtual squark states. For gluino lifetimes beyond a picosecond, the gluino hadronizes and forms a bound colour-singlet state containing the gluino and quarks or gluons [22], known as an R-hadron, before eventually decaying to a quark-antiquark pair and the $\widetilde{\chi}_1^0$. The long-lived gluino can lead to final states with significant $\vec{p}_{\mathrm{T}}^{\mathrm{miss}}$ from the undetected $\widetilde{\chi}_1^0$ particles and to jets with vertices located a significant distance (i.e. displaced) from the luminous region of the proton beams. A metastable gluino, with a decay length significantly beyond the scale of the CMS detector, can escape undetected.

This paper presents a search for new-physics processes in final states with one or more energetic jets and significant $\vec{p}_{\mathrm{T}}^{\mathrm{miss}}$. The search is performed with a sample of proton-proton (pp) collision data at a centre-of-mass energy of 13 TeV recorded by the CMS experiment in 2016. The analysed data sample corresponds to an integrated luminosity of $35.9 \pm 0.9\,\mathrm{fb}^{-1}$ [23]. Earlier searches using the same technique have been performed in pp collisions at $\sqrt{s} = 7$, 8, and 13 TeV by the CMS Collaboration [24–29]. The data set analysed in this analysis is a factor of 16 larger than that presented in ref. [29]. The search strategy aims to provide sensitivity to a broad range of SUSY-inspired models that predict the existence of a DM candidate, and the search is used to constrain the parameter spaces of a number of simplified SUSY models [30–32]. The overwhelmingly dominant background for a new-physics search in all-jet final states resulting from pp collisions is the production of multijet events via the strong interaction, a manifestation of quantum chromodynamics (QCD). Several dedicated variables are employed to suppress the multijet background to a negligible level while maintaining low kinematical thresholds and high experimental acceptance for final states characterized by the presence of significant $\vec{p}_{\mathrm{T}}^{\mathrm{miss}}$. Signal extraction is performed using additional kinematical variables, namely the number of jets, the number of jets identified as originating from bottom quarks, and the scalar and vector sums of the jet transverse momenta. The ATLAS and CMS Collaborations have performed similar searches in all-jet final states at $\sqrt{s} = 13$ TeV, of which those providing the tightest constraints are described in refs. [33–35]. This search does not employ specialized reconstruction techniques [36–46] that target long-lived gluinos.

This paper is organized as follows. Section 2 describes the CMS apparatus and the event reconstruction algorithms. Section 3 summarizes the selection criteria used to identify and categorize signal events and samples of control data. Section 4 outlines the various software packages used to generate the samples of simulated events. Sections 5 and 6 describe the methods used to estimate the background contributions from SM processes. The

results and interpretations are described in sections 7 and 8, respectively, and summarized in section 9.

2   The CMS detector and event reconstruction

The central feature of the CMS detector is a superconducting solenoid of 6 m internal diameter, providing a magnetic field of 3.8 T. Within the solenoid volume are a silicon pixel and strip tracker, a lead tungstate crystal electromagnetic calorimeter (ECAL), and a brass and scintillator hadron calorimeter (HCAL), each composed of a barrel and two endcap sections. Forward calorimeters extend the pseudorapidity coverage provided by the barrel and endcap detectors. Muons are detected in gas-ionization chambers embedded in the steel flux-return yoke outside the solenoid. A more detailed description of the CMS detector, together with a definition of the coordinate system used and the relevant kinematical variables, can be found in ref. [47].

Events of interest are selected using a two-tiered trigger system [48]. The first level, composed of custom hardware processors, uses information from the calorimeters and muon detectors to select events at a rate of around 100 kHz within a time interval of less than 4 μs. The second level, known as the high-level trigger, consists of a farm of processors running a version of the full event reconstruction software optimized for fast processing, and reduces the event rate to less than 1 kHz before data storage. The trigger logic used by this search is summarized in section 3.

The particle-flow (PF) event algorithm [49] reconstructs and identifies each individual particle with an optimized combination of information from the various elements of the CMS detector. In this process, the identification of the particle type (photon, electron, muon, charged hadron, neutral hadron) plays an important role in the determination of the particle direction and energy. The energy of photons [50] is directly obtained from the ECAL measurement, corrected for zero-suppression effects. The energy of electrons [51] is determined from a combination of the electron momentum at the primary interaction vertex as determined by the tracker, the energy of the corresponding ECAL measurement, and the energy sum of all bremsstrahlung photons spatially compatible with originating from the electron track. The energy of muons [52] is obtained from the curvature of the corresponding track. The energy of charged hadrons is determined from a combination of their momentum measured in the tracker and the matching ECAL and HCAL energy deposits, corrected for zero-suppression effects and for the response function of the calorimeters to hadronic showers. Finally, the energy of neutral hadrons is obtained from the corresponding corrected ECAL and HCAL energy. The reconstruction techniques used by this search are not specialized to target specific experimental signatures (such as displaced jets). The physics objects used in this search are defined below and are summarized in table 1. In the case of photons and leptons, further details can be found in ref. [29] and references therein.

The reconstructed vertex with the largest value of summed physics object p_T^2 is taken to be the primary pp interaction vertex (PV). The physics objects considered are those returned by a jet finding algorithm [53, 54] applied to all charged particle tracks associated with the vertex, and the associated p_T^{miss}, taken as the negative vector sum of the p_T of

Physics object acceptances	
Jet	$p_T > 40\,\text{GeV}$, $|\eta| < 2.4$
Photon	$p_T > 25\,\text{GeV}$, $|\eta| < 2.5$, isolated in cone $\Delta R < 0.3$
Electron	$p_T > 10\,\text{GeV}$, $|\eta| < 2.5$, $I^{\text{rel}} < 0.1$ in cone $0.05 < \Delta R(p_T) < 0.2$
Muon	$p_T > 10\,\text{GeV}$, $|\eta| < 2.5$, $I^{\text{rel}} < 0.2$ in cone $0.05 < \Delta R(p_T) < 0.2$
Single isolated track (SIT)	$p_T > 10\,\text{GeV}$, $|\eta| < 2.5$, $I^{\text{track}} < 0.1$ in cone $\Delta R < 0.3$
Baseline event selection	
All-jet final state	Veto events containing photons, electrons, muons, and SITs within acceptance
p_T^{miss} quality	Veto events based on filters related to beam and instrumental effects
Jet quality	Veto events containing jets that fail identification criteria or $0.1 < f_{h^\pm}^{j_1} < 0.95$
Jet energy and sums	$p_T^{j_1} > 100\,\text{GeV}$, $H_T > 200\,\text{GeV}$, $H_T^{\text{miss}} > 200\,\text{GeV}$
Jets outside acceptance	$H_T^{\text{miss}}/p_T^{\text{miss}} < 1.25$, veto events containing jets with $p_T > 40\,\text{GeV}$ and $|\eta| > 2.4$
Signal region	Baseline selection +
α_T threshold (H_T range)	0.65 (200–250 GeV), 0.60 (250–300), 0.55 (300–350), 0.53 (350–400), 0.52 (400–900)
$\Delta\phi_{\text{min}}^*$ threshold	$\Delta\phi_{\text{min}}^* > 0.5$ ($n_{\text{jet}} \geq 2$), $\Delta\phi_{\text{min}}^{*25} > 0.5$ ($n_{\text{jet}} = 1$)
Nominal categorization schema	
n_{jet}	1 (monojet)
	$\geq 2a$ (a denotes asymmetric, $40 < p_T^{j_2} < 100\,\text{GeV}$)
	2, 3, 4, 5, ≥ 6 (symmetric, $p_T^{j_2} > 100\,\text{GeV}$)
n_b	0, 1, 2, 3, ≥ 4 (can be dropped/merged vs. n_{jet})
H_T boundaries	200, 400, 600, 900, 1200 GeV (can be dropped/merged vs. n_{jet}, n_b)
H_T^{miss} boundaries	200, 400, 600, 900 GeV (can be dropped/merged vs. n_{jet}, n_b, H_T)
Simplified categorization schema	
Topology (n_{jet}, n_b)	Monojet-like $(1 \cap {\geq} 2a, 0)$, $(1 \cap {\geq} 2a, {\geq} 1)$
	Low n_{jet} $(2 \cap 3, 0 \cap 1)$, $(2 \cap 3, {\geq} 2)$
	Medium n_{jet} $(4 \cap 5, 0 \cap 1)$, $(4 \cap 5, {\geq} 2)$
	High n_{jet} $({\geq} 6, 0 \cap 1)$, $({\geq} 6, {\geq} 2)$
H_T boundaries	$H_T > 200\,\text{GeV}$ ($n_{\text{jet}} \leq 3$), $H_T > 400\,\text{GeV}$ ($n_{\text{jet}} \geq 4$)
H_T^{miss} boundaries	200, 400, 600, 900 GeV
Control regions	Baseline selection +
μ+jets (inverted μ veto)	$p_T^{\mu_1} > 30\,\text{GeV}$, $|\eta^{\mu_1}| < 2.1$, $\Delta R(\mu, j_i) > 0.5$, $30 < m_T(\vec{p}_T^{\,\mu}, \vec{p}_T^{\text{miss}}) < 125\,\text{GeV}$
$\mu\mu$+jets (inverted μ veto)	$p_T^{\mu_{1,2}} > 30\,\text{GeV}$, $|\eta^{\mu_{1,2}}| < 2.1$, $\Delta R(\mu_{1,2}, j_i) > 0.5$, $|m_{\mu\mu} - m_Z| < 25\,\text{GeV}$
Multijet-enriched	Sidebands to signal region: $H_T^{\text{miss}}/p_T^{\text{miss}} > 1.25$ and/or $\Delta\phi_{\text{min}}^* < 0.5$

Table 1. Summary of the physics object acceptances, the baseline event selection, the signal and control regions, and the event categorization schemas. The nominal categorization schema is defined in full in appendix A.

those physics objects. Charged particle tracks associated with vertices from additional pp interactions within the same or nearby bunch crossings (pileup) are not considered by the PF algorithm as part of the global event reconstruction. The energy deposit associated with each physics object is corrected to account for contributions from neutral particles originating from pileup interactions [55].

Samples of signal events and control data are defined, respectively, by the absence or presence of photons and leptons that are isolated from other activity in the event. Photons are required to be isolated [50] within a cone around the photon trajectory defined by the radius $\Delta R = \sqrt{(\Delta\phi)^2 + (\Delta\eta)^2} = 0.3$, where $\Delta\phi$ and $\Delta\eta$ represent differences in the azimuthal angle (radians) and pseudorapidity. Isolation for an electron or muon is a relative quantity, I^{rel}, defined as the scalar p_{T} sum of all PF particle candidates within a cone around its trajectory, divided by the lepton p_{T}. The cone radius is dependent on the lepton p_{T}, $\Delta R = \min[\max(0.05, 10\,\mathrm{GeV}/p_{\mathrm{T}}), 0.2]$, to maintain high efficiency for semileptonic decays of Lorentz-boosted top quarks [56]. Isolated electrons and muons are required to satisfy $I^{\mathrm{rel}} < 0.1$ and 0.2, respectively. Electron and muon candidates that fail any of the aforementioned requirements, as well as charged-hadron candidates from hadronically decaying tau leptons, are collectively labelled as single isolated tracks (SITs) if the scalar p_{T} sum of additional tracks associated with the PV within a cone $\Delta R < 0.3$ around the track trajectory, relative to the track p_{T}, satisfies $I^{\mathrm{track}} < 0.1$. All isolation variables exclude the contributions from the physics object itself and pileup interactions [50–52]. The experimental acceptances for photons, electrons, muons, and SITs are defined by the transverse momentum requirements $p_{\mathrm{T}} > 25$, 10, 10, and 10 GeV, respectively, and the pseudorapidity requirement $|\eta| < 2.5$.

Jets are reconstructed from the PF particle candidates, clustered by the anti-k_{T} algorithm [53, 54] with a distance parameter of 0.4. In this process, the raw jet energy is obtained from the sum of the particle candidate energies, and the raw jet momentum by the vectorial sum of the particle candidate momenta, which results in a nonzero jet mass. An offset correction is applied to jet energies to take into account the contributions from neutral particles produced in pileup interactions [55, 57]. The raw jet energies are then corrected to establish a relative uniform response of the calorimeter in η and a calibrated absolute response in p_{T}. Jet energy corrections are derived from simulation, and are confirmed with in situ measurements of the energy balance in dijet, multijet, γ+jets, and leptonically decaying Z+jets events [58]. Jets are required to satisfy $p_{\mathrm{T}} > 40$ GeV and $|\eta| < 2.4$. Jets are also subjected to a standard set of identification criteria [59] that require each jet to contain at least two particle candidates and at least one charged particle track, and the energy fraction $f_{\mathrm{h}^\pm}$ attributed to charged-hadron particle candidates is required to be nonzero.

Jets can be identified as originating from b quarks using the combined secondary vertex (CSVv2) algorithm [60]. Data samples are used to measure the b tagging efficiency, which is the probability to correctly identify jets originating from b quarks, as well as the mistag probabilities for jets that originate from light-flavour (LF) partons (u, d, s quarks or gluon) or a charm quark. A working point is employed that yields a b tagging efficiency of $\approx$69% for jets with $p_{\mathrm{T}} > 30$ GeV from $\mathrm{t\bar{t}}$ events, and charm and LF mistag probabilities of $\approx$18 and $\approx$1%, respectively, for multijet events.

Finally, the most accurate estimator for $\vec{p}_{\mathrm{T}}^{\,\mathrm{miss}}$ is defined as the projection on the plane perpendicular to the beams of the negative vector sum of the momenta of all PF particle candidates in an event. Its magnitude is referred to as $p_{\mathrm{T}}^{\mathrm{miss}}$.

3 Event selection and categorization

A baseline set of event selection criteria, described in section 3.1, is used as a basis for all data samples used in this search. Two additional requirements, described in section 3.2, are employed to define a sample of signal events, labelled henceforth as the signal region (SR). The categorization of signal events and the background composition are described in sections 3.3 and 3.4, respectively. Three independent control regions (CRs), comprising large samples of event data, are defined by the selection criteria described in section 3.5. All selection criteria are summarized in table 1.

3.1 Baseline selections

Events containing isolated photons, electrons and muons, or SITs that satisfy the requirements summarized in table 1 are vetoed. The aforementioned vetoes are employed to select all-jet final states, suppress SM processes that produce final states containing neutrinos, and reduce backgrounds from misreconstructed or nonisolated leptons as well as single-prong hadronic decays of τ leptons.

Beam halo, spurious jet-like features originating from isolated noise patterns in the calorimeter systems, detector inefficiencies, and reconstruction failures can all lead to large values of $p_{\mathrm{T}}^{\mathrm{miss}}$. Such events are rejected with high efficiency using dedicated vetoes [61, 62]. Events are vetoed if any jet fails the identification criteria described in section 2. Further, $f_{\mathrm{h}\pm}$ for the highest p_{T} jet of the event, $\mathrm{j_1}$, is required to satisfy $0.1 < f_{\mathrm{h}\pm}^{\mathrm{j_1}} < 0.95$ to further suppress beam halo and rare reconstruction failures.

The highest p_{T} jet in the event is required to satisfy $p_{\mathrm{T}}^{\mathrm{j_1}} > 100\,\mathrm{GeV}$. The mass scale of each event is estimated from the scalar p_{T} sum of the jets, defined as $H_{\mathrm{T}} = \sum_{\mathrm{j_i}=1}^{n_{\mathrm{jet}}} p_{\mathrm{T}}^{\mathrm{j_i}}$, where n_{jet} is the number of jets within the experimental acceptance. The estimator for $\vec{p}_{\mathrm{T}}^{\mathrm{miss}}$ used by this search is given by the magnitude of the vector p_{T} sum of the jets, $H_{\mathrm{T}}^{\mathrm{miss}} = |\sum_{\mathrm{j_i}=1}^{n_{\mathrm{jet}}} \vec{p}_{\mathrm{T}}^{\mathrm{j_i}}|$. Significant hadronic activity and $\vec{p}_{\mathrm{T}}^{\mathrm{miss}}$, typical of SUSY processes, is ensured by requiring $H_{\mathrm{T}} > 200\,\mathrm{GeV}$ and $H_{\mathrm{T}}^{\mathrm{miss}} > 200\,\mathrm{GeV}$, respectively.

Events are vetoed if any additional jet satisfies $p_{\mathrm{T}} > 40\,\mathrm{GeV}$ and $|\eta| > 2.4$ to maintain the resolution of the $H_{\mathrm{T}}^{\mathrm{miss}}$ variable. An additional veto is employed to deal with the circumstance in which several jets with transverse momentum below the p_{T} thresholds and collinear in ϕ can result in significant $H_{\mathrm{T}}^{\mathrm{miss}}$ relative to $p_{\mathrm{T}}^{\mathrm{miss}}$, the latter of which is less sensitive to jet thresholds. This type of event topology, which is typical of multijet events, is suppressed while maintaining high efficiency for new-physics processes with significant $\vec{p}_{\mathrm{T}}^{\mathrm{miss}}$ by requiring $H_{\mathrm{T}}^{\mathrm{miss}}/p_{\mathrm{T}}^{\mathrm{miss}} < 1.25$.

3.2 Signal region

The multijet background dominates over all other SM backgrounds following the application of the baseline event selection criteria. The multijet background is suppressed to a negligible level through the application of two dedicated variables that provide strong discrimination between multijet events with $\vec{p}_{\mathrm{T}}^{\mathrm{miss}}$ resulting from instrumental sources, such as jet energy mismeasurements, and new-physics processes that involve the production of weakly interacting particles that escape detection.

The first variable, α_{T} [24, 63], is designed to be intrinsically robust against jet energy mismeasurements. In its simplest form, the α_{T} variable is defined as $\alpha_{\mathrm{T}} = E_{\mathrm{T}}^{\mathrm{j2}}/M_{\mathrm{T}}$, where $M_{\mathrm{T}} = \sqrt{2E_{\mathrm{T}}^{\mathrm{j1}} E_{\mathrm{T}}^{\mathrm{j2}}(1 - \cos\phi_{\mathrm{j_1,j_2}})}$ and $\phi_{\mathrm{j_1,j_2}}$ is defined as the azimuthal angle between jets $\mathrm{j_1}$ and $\mathrm{j_2}$. In the absence of jet energy mismeasurements, and in the limit for which the E_{T} of each jet is large compared with its mass, a well-measured dijet event with $E_{\mathrm{T}}^{\mathrm{j1}} = E_{\mathrm{T}}^{\mathrm{j2}}$ and back-to-back jets ($\phi_{\mathrm{j_1,j_2}} = \pi$) yields an α_{T} value of 0.5. In the presence of a jet energy mismeasurement, $E_{\mathrm{T}}^{\mathrm{j1}} > E_{\mathrm{T}}^{\mathrm{j2}}$ and $\alpha_{\mathrm{T}} < 0.5$. Values significantly greater than 0.5 can be observed when the two jets are not back-to-back and recoil against $\vec{p}_{\mathrm{T}}^{\mathrm{miss}}$ from weakly interacting particles that escape the detector. The definition of the α_{T} variable can be generalized for events with two or more jets, as described in ref. [24]. Multijet events populate the region $\alpha_{\mathrm{T}} \lesssim 0.5$ and the α_{T} distribution is characterized by a sharp edge at 0.5, beyond which the multijet event yield falls by several orders of magnitude. The SM backgrounds that involve the production of neutrinos result in a long tail in α_{T} beyond values of 0.5. A H_{T}-dependent α_{T} threshold that decreases from 0.65 at low H_{T} to 0.52 at high H_{T} within the range $200 < H_{\mathrm{T}} < 900\,\mathrm{GeV}$ is employed to maintain an approximately constant rejection power against the multijet background.

The second variable, known as $\Delta\phi_{\mathrm{min}}^*$, considers the minimum azimuthal angular separation between each jet in the event and the vector p_{T} sum of all other jets in the event. Multijet events typically populate the region $\Delta\phi_{\mathrm{min}}^* \approx 0$ while events with genuine $\vec{p}_{\mathrm{T}}^{\mathrm{miss}}$ can have values up to $\Delta\phi_{\mathrm{min}}^* = \pi$. The requirement $\Delta\phi_{\mathrm{min}}^* > 0.5$ is sufficient to reduce significantly the multijet background, including rare contributions from energetic multijet events that yield both high jet multiplicities and significant $\vec{p}_{\mathrm{T}}^{\mathrm{miss}}$ because of high-multiplicity neutrino production in semileptonic heavy-flavour decays. For events that satisfy $n_{\mathrm{jet}} = 1$, a small modification to the $\Delta\phi_{\mathrm{min}}^*$ variable is utilized that considers any additional jets with $25 < p_{\mathrm{T}} < 40\,\mathrm{GeV}$ that are outside the nominal experimental acceptance ($\Delta\phi_{\mathrm{min}}^{*\,25} > 0.5$).

The requirements on α_{T} and $\Delta\phi_{\mathrm{min}}^*$, summarized in table 1, suppress the expected contribution from multijet events to the sub-percent level with respect to the total expected background counts from all other SM processes. For the region $H_{\mathrm{T}} > 900\,\mathrm{GeV}$, the necessary control of the multijet background is achieved solely with the $\Delta\phi_{\mathrm{min}}^*$ and $\Delta\phi_{\mathrm{min}}^{*\,25}$ variables. These requirements complete the definition of the SR.

Signal events are recorded with a number of trigger algorithms. Events with $n_{\mathrm{jet}} \geq 2$ must satisfy thresholds on both H_{T} and α_{T} that are looser than those used to define the SR. High-activity events that satisfy $H_{\mathrm{T}} > 900\,\mathrm{GeV}$ are also recorded. Finally, a trigger condition that requires $H_{\mathrm{T}}^{\mathrm{miss}} > 120\,\mathrm{GeV}$, $p_{\mathrm{T}}^{\mathrm{miss}} > 120\,\mathrm{GeV}$, and a single jet with $p_{\mathrm{T}} > 20\,\mathrm{GeV}$ and $|\eta| < 5.2$ is also used to efficiently record signal events for all categories of the SR, including those that satisfy $n_{\mathrm{jet}} \geq 1$. The combined performance of these trigger algorithms yields high efficiencies, as determined from samples of CR data enriched in vector boson $+$ jets and $t\bar{t}$ events. The efficiencies are primarily H_{T}-dependent and range from 97.4–97.9% ($200 < H_{\mathrm{T}} < 600\,\mathrm{GeV}$) to 100% ($H_{\mathrm{T}} > 600\,\mathrm{GeV}$) with statistical and systematic uncertainties at the percent level. Trigger efficiencies for a range of benchmark signal models are typically comparable or higher ($\approx$100%).

3.3 Event categorization

Signal events are categorized into 27 discrete topologies according to $n_{\rm jet}$ and the number of b-tagged jets $n_{\rm b}$. Events are further binned according to the energy sums $H_{\rm T}$ and $H_{\rm T}^{\rm miss}$. The binning schema, defined in full in table 6 (appendix A), is determined primarily by the statistical power of the μ+jets and $\mu\mu$+jets CRs.

Seven bins in $n_{\rm jet}$ are considered, as summarized in table 1. Events that contain only a single jet within the experimental acceptance ($n_{\rm jet} = 1$) are labelled as "monojet". Events containing two or more jets are categorized according to the second-highest jet $p_{\rm T}$. Events that satisfy $n_{\rm jet} \geq 2$ with only the highest $p_{\rm T}$ jet satisfying $p_{\rm T} > 100\,{\rm GeV}$ are labelled as "asymmetric". Events for which the second-highest jet $p_{\rm T}$ also satisfies $p_{\rm T} > 100\,{\rm GeV}$ are labelled as "symmetric" and are categorized according to $n_{\rm jet}$ (2, 3, 4, 5, and $\geq$6). The symmetric topology targets the pair production of SUSY particles and their prompt cascade decays, while the monojet and asymmetric topologies preferentially target models with a compressed mass spectrum and long-lived SUSY particles.

Events are also categorized according to $n_{\rm b}$ (0, 1, 2, 3, $\geq$4), where $n_{\rm b}$ is bounded from above by $n_{\rm jet}$ and the choice of categorization is dependent on $n_{\rm jet}$. Higher $n_{\rm b}$ multiplicities target the production of third-generation squarks.

The nominal binning schema for $H_{\rm T}$ is defined as follows: four bounded bins that satisfy 200–400, 400–600, 600–900, and 900–1200 GeV, and a final open bin $H_{\rm T} > 1200\,{\rm GeV}$. This schema is adapted per ($n_{\rm jet}$, $n_{\rm b}$) category as follows: only the region $H_{\rm T} > 400\,{\rm GeV}$ is considered for events that satisfy $n_{\rm jet} \geq 4$, and bins at high $H_{\rm T}$ are merged with lower-$H_{\rm T}$ bins to satisfy a threshold of at least four events in the corresponding bins of the CRs.

The $H_{\rm T}^{\rm miss}$ variable is used to further categorize events according to three bounded bins that satisfy 200–400, 400–600, and 600–900, and a final open bin $H_{\rm T}^{\rm miss} > 900\,{\rm GeV}$. The $H_{\rm T}^{\rm miss}$ binning depends on $n_{\rm jet}$, $n_{\rm b}$, and $H_{\rm T}$. Given that $H_{\rm T}^{\rm miss}$ cannot exceed $H_{\rm T}$ by construction, the lower bound of the final $H_{\rm T}^{\rm miss}$ bin is restricted to be not higher than the lower bound of the $H_{\rm T}$ bin in question. Events that satisfy $n_{\rm jet} = 1$ or $200 < H_{\rm T} < 400\,{\rm GeV}$ are not categorized according to $H_{\rm T}^{\rm miss}$.

In total, there are 254 bins in the SR. An alternate, simplified binning schema is also provided in which events are categorized according to eight topologies defined in terms of $n_{\rm jet}$ and $n_{\rm b}$. For each topology, event yields are integrated over the full available $H_{\rm T}$ range and categorized according to the four nominal $H_{\rm T}^{\rm miss}$ bins defined above. This schema has 32 bins that are exclusive, contiguous, and provide a complete coverage of the SR. The SM background estimates are obtained from the same likelihood model as the one used to determine the nominal result.

3.4 Background composition

Following the application of the SR selection criteria, the multijet background is reduced to a negligible level. The remaining background contributions are dominated by processes that involve the production of high-$p_{\rm T}$ neutrinos in the final state. The associated production of jets and a Z boson that decays to $\nu\bar{\nu}$ dominates the background contributions for events containing low numbers of jets and b-tagged jets. The $Z(\to \nu\bar{\nu})$+jets background is irreducible.

The associated production of jets and a W boson that decays to $\ell\nu$ ($\ell = $ e, μ, τ) is also a significant background in the same phase space. The production and semileptonic decay of top quark-antiquark pairs ($t\bar{t}$) becomes the dominant background process for events containing high numbers of jets or b-tagged jets. Events that contain the leptonic decay of a W boson are typically rejected by the vetoes that identify the presence of leptons or single isolated tracks. If the lepton is outside the experimental acceptance, or is not identified or isolated, then the event is not vetoed and the aforementioned processes lead to what is collectively known as the "lost lepton" ($\ell_{\rm lost}$) background. Residual contributions from other SM processes are also considered, such as single top quark production; WW, WZ, ZZ (diboson) production; and the associated production of $t\bar{t}$ and a boson ($t\bar{t}$W, $t\bar{t}$Z, $t\bar{t}\gamma$, and $t\bar{t}$H).

3.5 Control regions

Topological and kinematical requirements, summarized in table 1, ensure that the samples of CR data are enriched in the same or similar SM processes that populate the SR, as well as being depleted in contributions from SUSY processes (signal contamination).

Three sidebands to the SR comprising multijet-enriched event samples are defined by: $1.25 < H_{\rm T}^{\rm miss}/p_{\rm T}^{\rm miss} < 3.0$ (region A), $0.2 < \Delta\phi_{\rm min}^* < 0.5$ (B), and both $1.25 < H_{\rm T}^{\rm miss}/p_{\rm T}^{\rm miss} < 3.0$ and $0.2 < \Delta\phi_{\rm min}^* < 0.5$ (C). Events are categorized according to $n_{\rm jet}$ and $H_{\rm T}$, identically to the SR. Events are recorded with the signal triggers described above.

Two additional CRs comprising μ+jets and $\mu\mu$+jets event samples are defined by the application of the baseline selections and requirements on isolated, central, high-$p_{\rm T}$ muons. Tighter isolation requirements for the muons are applied with respect to those indicated in table 1. A trigger condition that requires an isolated muon with $p_{\rm T} > 24\,\rm GeV$ and $|\eta| < 2.1$ is used to record the μ+jets and $\mu\mu$+jets event samples with efficiencies of $\approx$90 and $\approx$99%, respectively. For both samples, no requirements on $\alpha_{\rm T}$ or $\Delta\phi_{\rm min}^*$ are imposed. The kinematical properties of events in the μ+jets and $\mu\mu$+jets CRs and SR are comparable once the muon or dimuon system is ignored in the calculation of event-level quantities such as $H_{\rm T}$ and $H_{\rm T}^{\rm miss}$. Events in both samples are categorized according to $n_{\rm jet}$, $H_{\rm T}$, and $n_{\rm b}$, with counts integrated over $H_{\rm T}^{\rm miss}$. The $n_{\rm jet}$ categorization is identical to the SR. Background predictions are determined using up to eleven bins in $H_{\rm T}$ that are then aggregated to match the $H_{\rm T}$ binning schema used by the SR. The $n_{\rm b}$ categorization for μ+jets events is identical to the SR, whereas $\mu\mu$+jets events are subdivided according to $n_{\rm b} = 0$ and $n_{\rm b} \geq 1$. Differences in the binning schemas between the SR and CRs are accounted for in the background estimation methods through simulation-based templates, the modelling of which is validated against control data.

The μ+jets event sample is enriched in events from W($\to \mu\nu$)+jets and $t\bar{t}$ production, as well as other SM processes (e.g. single top quark and diboson production), that are manifest in the SR as the $\ell_{\rm lost}$ backgrounds. Each event is required to contain a single isolated muon with $p_{\rm T} > 30\,\rm GeV$ and $|\eta| < 2.1$ to satisfy trigger conditions, and is well separated from each jet j_i in the event according to $\Delta R(\mu, j_i) > 0.5$. The transverse mass $m_{\rm T} = \sqrt{2p_{\rm T}^\mu p_{\rm T}^{\rm miss}[1 - \cos(\Delta\phi_{\mu, \vec{p}_{\rm T}^{\rm miss}})]}$, where $\Delta\phi_{\mu, \vec{p}_{\rm T}^{\rm miss}}$ is the difference between the azimuthal angles of the muon transverse momentum vector $\vec{p}_{\rm T}^\mu$ and of $\vec{p}_{\rm T}^{\rm miss}$, must fall within the range 30–125 GeV to select a sample of events rich in W bosons.

The $\mu\mu$+jets sample is enriched in $Z \to \mu^+\mu^-$ events that have similar acceptance and kinematical properties to $Z(\to \nu\bar{\nu})$+jets events when the muons are ignored. The sample uses selection criteria similar to the μ+jets sample, but requires two oppositely charged, isolated muons that both satisfy $p_T > 30\,\text{GeV}$, $|\eta| < 2.1$, and $\Delta R(\mu_{1,2}, j_i) > 0.5$. The muons are also required to have a dilepton invariant mass $m_{\mu\mu}$ within a $\pm 25\,\text{GeV}$ window around the mass of the Z boson [12].

4   Monte Carlo simulation

The search relies on several samples of simulated events, produced with Monte Carlo (MC) generator programs, to aid the estimation of SM backgrounds and evaluate potential signal contributions.

The MadGraph5_aMC@NLO 2.2.2 [64] event generator is used at leading-order (LO) accuracy to produce samples of W+jets, Z+jets, $t\bar{t}$, and multijet events. Up to three or four additional partons are included in the matrix-element calculation for $t\bar{t}$ and vector boson production, respectively. Simulated W+jets and Z+jets events are weighted according to the true vector boson p_T to account for the effect of missing next-to-leading-order (NLO) QCD and EW terms in the matrix-element calculation [64, 65], according to the method described in ref. [66]. Within the range of vector boson p_T that can be probed by this search, the QCD and EW corrections [65] are largest, $\approx 40\%$ and $\approx 15\%$, at low and high values of boson p_T, respectively. Simulated $t\bar{t}$ events are weighted to improve the description of jets arising from initial-state radiation (ISR) [67]. The weights vary from 0.92 to 0.51 depending on the number of jets (1–6) from ISR, with an uncertainty of one half the deviation from unity. The MadGraph5_aMC@NLO generator is used at NLO accuracy to generate samples of s-channel production of single top quark, as well as $t\bar{t}W$ and $t\bar{t}Z$ events. The NLO powheg v2 [68, 69] generator is used to describe the t- and Wt-channel production of events containing single top quarks, as well as $t\bar{t}H$ events. The pythia 8.205 [70] program is used to generate diboson (WW, WZ, ZZ) production.

Event samples for signal models involving the production of gluino or squark pairs, in association with up to two additional partons, are generated at LO with MadGraph5_aMC@NLO, and the decay of the SUSY particles is performed with the pythia program. The NNPDF3.0 LO and NNPDF3.0 NLO [71] parton distribution functions (PDFs) are used, respectively, with the LO and NLO generators described above.

The simulated samples for SM processes are normalized according to production cross sections that are calculated with NLO and next-to-NLO precision [64, 69, 72–76]. The production cross sections for pairs of gluinos or squarks are determined at NLO plus next-to-leading-logarithm (NLL) precision [77–82]. All other SUSY particles, apart from the $\widetilde{\chi}_1^0$, are assumed to be heavy and decoupled from the interaction. Uncertainties in the cross sections are determined from different choices of PDF sets, and factorization and renormalization scales (μ_F and μ_R), according to the prescription in ref. [82]. The pythia program with the CUETP8M1 tune [83, 84] is used to describe parton showering and hadronization for all simulated samples.

The RHADRONS package within the PYTHIA 8.205 program is used to describe the formation of R-hadrons through the hadronization of gluinos [22, 85, 86]. The hadronization process, steered according to the default parameter settings of the RHADRONS package, predominantly yields meson-like ($\widetilde{g}q\overline{q}$) and baryon-like ($\widetilde{g}qqq$) states, as well as glueball-like ($\widetilde{g}g$) states with a probability $P_{\widetilde{g}g} = 10\%$, where $\widetilde{g}$, g, q, and $\overline{q}$ represent a gluino, gluon, quark, and antiquark, respectively. The gluino is assumed to undergo a three-body decay, to a $q\overline{q}$ pair and the $\widetilde{\chi}_1^0$, according to its proper decay length $c\tau_0$ that is a parameter of the simplified model [87]. Studies with alternative values for parameters that influence the hadronization of the gluino, such as $P_{\widetilde{g}g} = 50\%$, indicate a minimal influence on the event topology and kinematical variables for the models considered in this paper. Further, the model-dependent interactions of R-hadrons with the detector material are not considered by default, as studies demonstrate that the sensitivity of this search is only moderately dependent on these interactions, as discussed in section 8.

The description of the detector response is implemented using the GEANT4 [88] package for all simulated SM processes. Scale factors are applied to simulated event samples that correct for differences with respect to data in the b tagging efficiency and mistag probabilities. The scale factors have typical values of $\approx$0.95–1.00 and $\approx$1.00–1.20, respectively, for a jet p_T range of 40–600 GeV [60]. All remaining signal models rely on the CMS fast simulation package [89] that provides a description that is consistent with GEANT4 following the application of near-unity corrections for the differences in the b tagging efficiency and mistag probabilities, as well as corrections for the differences in the modelling of the H_T^{miss} distribution. To model the effects of pileup, all simulated events are generated with a nominal distribution of pp interactions per bunch crossing and then weighted to match the pileup distribution as measured in data.

5   Nonmultijet background estimation

The ℓ_{lost} and $Z(\to \nu\overline{\nu})$+jets backgrounds, collectively labelled henceforth as the nonmultijet backgrounds, are estimated from data samples in CRs and transfer factors $\mathcal{R}$ determined from the ratios of expected counts obtained from simulation:

$$\mathcal{R}^{\ell_{lost}} = \frac{N_{MC}^{\ell_{lost}}(n_{jet}, H_T, n_b, H_T^{miss})}{N_{MC}^{\mu+jets}(n_{jet}, H_T, n_b)}, \qquad N_{pred}^{\ell_{lost}} = \mathcal{R}^{\ell_{lost}} \, N_{data}^{\mu+jets}, \qquad (5.1)$$

$$\mathcal{R}^{Z\to\nu\overline{\nu}} = \frac{N_{MC}^{Z\to\nu\overline{\nu}}(n_{jet}, H_T, n_b, H_T^{miss})}{N_{MC}^{\mu\mu+jets}(n_{jet}, H_T, n_b)}, \qquad N_{pred}^{Z\to\nu\overline{\nu}} = \mathcal{R}^{Z\to\nu\overline{\nu}} \, N_{data}^{\mu\mu+jets}, \qquad (5.2)$$

where $\mathcal{R}^{\ell_{lost}}$ and $\mathcal{R}^{Z\to\nu\overline{\nu}}$ are the transfer factors that act as multiplier terms on the event counts $N_{data}^{\mu+jets}$ and $N_{data}^{\mu\mu+jets}$ observed in each (n_{jet}, H_T, n_b) bin of, respectively, the μ+jets and $\mu\mu$+jets CRs to estimate the ℓ_{lost} or $Z(\to \nu\overline{\nu})$+jets background counts $N_{pred}^{\ell_{lost}}$ and $N_{pred}^{Z\to\nu\overline{\nu}}$ in the corresponding (n_{jet}, H_T, n_b, H_T^{miss}) bins of the SR. Several sources of uncertainty in the transfer factors are evaluated. In addition to statistical uncertainties arising from finite-size simulated event samples, the most relevant systematic effects are discussed below.

The uncertainties from known theoretical and experimental sources are propagated through to the transfer factors to ascertain the magnitude of variations related to the following: the jet energy scale, the scale factors related to the b tagging efficiency and mistag probabilities, the efficiency to trigger on and identify, or veto, well-reconstructed isolated leptons, the PDFs [90], μ_F and μ_R, and the modelling of jets from ISR produced in association with $t\bar{t}$ [67]. Uncertainties of 100% in both the NLO QCD and EW corrections to the W+jets and Z+jets simulated samples are also considered. A 5% uncertainty in the total inelastic cross section [91] is assumed and propagated through to the weighting procedure to account for differences between the data and simulation in the pileup distributions. Uncertainties in the signal trigger efficiency measurements are also propagated to the transfer factors. The effects of the aforementioned systematic uncertainties are summarized in table 2, in terms of representative ranges. Each source of uncertainty is assumed to vary with a fully correlated behaviour across the full phase space of the SR and CRs.

Sources of additional uncertainties are determined from closure tests performed using control data that aim to identify n_jet- or H_T-dependent sources of systematic bias arising from extrapolations in kinematical variables covered by the transfer factors. Several sets of tests are performed. The accuracy of the modelling of the efficiencies of both the α_T and $\Delta\phi^*_\mathrm{min}$ requirements is estimated from both the μ+jets and $\mu\mu$+jets samples. The effects of W boson polarization are probed by using μ+jets events with a positively charged muon to predict those containing a negatively charged muon. Finally, the efficiency of the single isolated track veto is also probed using a sample of μ+jets events. The uncertainties are summarized in table 2.

The simulation modelling of the n_b distributions for the $Z(\to\nu\bar{\nu})$+jets background in the region $n_\mathrm{b} \geq 1$ is evaluated through a binned maximum-likelihood fit to the observed n_b distributions in data in each (n_jet, H_T) bin of the $\mu\mu$+jets CR. Additional checks are performed in $\mu\mu$+jets samples that are enriched in mistagged jets that originate from LF partons or charm quarks, or the genuine tags of b quarks from gluon splitting, through the use of loose and tight working points of the b tagging algorithm, respectively. No tests reveal evidence of significant bias in the simulation modelling of the n_b distribution.

Finally, the modelling of the $H_\mathrm{T}^\mathrm{miss}$ distribution in simulated events is compared to the distributions observed in μ+jets and $\mu\mu$+jets control data, and inspected for trends, by assuming a linear behaviour of the ratio of observed and simulated counts as a function of $H_\mathrm{T}^\mathrm{miss}$. Linear fits are performed independently for each n_jet category while integrating event counts over n_b and H_T, and then repeated for each H_T bin while integrating event counts over n_jet and n_b. Systematic uncertainties are determined from any nonclosure between data and simulation as a function of n_jet and are assumed to be correlated in H_T (and n_b), and vice versa. The uncertainties can be as large as $\approx$50% in the most sensitive $H_\mathrm{T}^\mathrm{miss}$ bins.

6 Multijet background estimation

The multijet background is estimated using the three data sidebands defined in section 3.5. Events in each sideband are categorized according to n_jet and H_T. The event counts in data

Source of uncertainty	Magnitude [%]	
	ℓ_{lost}	$Z \to \nu\bar{\nu}$
Finite-size simulated samples	1–50	1–50
Total inelastic cross section (pileup)	0.6–3.8	2.3–2.8
μ_{F} and μ_{R} scales	2.3–3.6	0.9–4.7
Parton distribution functions	1.1–2.7	0.0–3.3
W+jets cross section	0.2–1.4	—
$t\bar{t}$ cross section	0.0–1.0	—
NLO QCD corrections	1.5–13	2.6–17
NLO EW corrections	0.1–9.5	0.0–7.8
ISR ($t\bar{t}$)	0.8–1.1	—
Signal trigger efficiency	0.0–3.1	0.0–2.0
Lepton efficiency (selection)	2.0	4.0
Lepton efficiency (veto)	5.0	5.0
Jet energy scale	3.4–5.5	5.3–8.0
b tagging efficiency	0.4–0.6	0.3–0.6
Mistag probabilities	0.1–1.4	0.2–1.8
α_{T} extrapolation	3–9, 2–6	3–9, 2–6
$\Delta\phi^*_{\text{min}}$ extrapolation	3–22, 2–18	3–22, 2–18
W boson polarization	1–7, 2–7	—
Single isolated track veto	0–10, 0–13	—

Table 2. Systematic uncertainties in the ℓ_{lost} and $Z \to \nu\bar{\nu}$ background evaluation. The quoted ranges are representative of the minimum and maximum variations observed across all bins of the signal region. Pairs of ranges are quoted for uncertainties determined from closure tests in data, which correspond to variations as a function of n_{jet} and H_{T}, respectively.

are corrected to account for contamination from nonmultijet SM processes, such as vector boson and $t\bar{t}$ production, as well as the residual contributions from other SM processes. The nonmultijet processes are estimated from the μ+jets and $\mu\mu$+jets CRs, following a procedure similar to the one described in section 5. The corrected counts are assumed to arise solely from multijet production. For each sideband, a transfer factor per (n_{jet}, H_{T}) bin is obtained from simulation, defined as the ratio of the number of multijet events that satisfies the SR requirements to the number that satisfies the sideband requirement. Estimates of the multijet background per (n_{jet}, H_{T}) bin are obtained per sideband from the product of the transfer factors and the corrected data counts.

The final estimate per (n_{jet}, H_{T}) bin is a weighted sum of the three estimates. The multijet background is found to be small, typically at the percent level, relative to the sum of all nonmultijet backgrounds in all (n_{jet}, n_{b}) bins of the SR. The $H_{\text{T}}^{\text{miss}}/p_{\text{T}}^{\text{miss}}$ and $\Delta\phi^*_{\text{min}}$

variables that are used to define the sidebands are determined to be only weakly correlated for multijet events, and the estimates from each sideband are assumed to be uncorrelated. Statistical uncertainties associated with the finite event counts in data and simulated event samples, as large as $\approx 100\%$, are propagated to each estimate. Uncertainties as large as $\approx 20\%$ in the estimates of nonmultijet contamination are also propagated to the corrected events. Any differences between the three estimates per $(n_{\text{jet}},\ H_{\text{T}})$ bin are adequately covered by systematic uncertainties of 100%, which are assumed to be uncorrelated across $(n_{\text{jet}},\ H_{\text{T}})$ bins.

A model is assumed to determine the estimates as a function of n_{b} and $H_{\text{T}}^{\text{miss}}$. The distribution of multijet events as a function of n_{b} and $H_{\text{T}}^{\text{miss}}$ per $(n_{\text{jet}},\ H_{\text{T}})$ bin is assumed to be identical to the distribution expected for the nonmultijet backgrounds. This assumption is based on simulation-based studies and is a valid simplification given the magnitude of the multijet background relative to the sum of all other SM backgrounds, as well as the magnitude of the statistical and systematic uncertainties in the estimates described above.

7 Results

A likelihood model is used to obtain the SM expectations in the SR and each CR, as well as to test for the presence of new-physics signals. The observed event count in each bin, defined in terms of the n_{jet}, n_{b}, H_{T}, and $H_{\text{T}}^{\text{miss}}$ variables, is modelled as a Poisson-distributed variable around the SM expectation and a potential signal contribution (assumed to be zero in the following discussion). The expected event counts from nonmultijet processes in the SR are related to those in the μ+jets and $\mu\mu$+jets CRs via simulation-based transfer factors, as described in section 5. The systematic uncertainties in the nonmultijet estimates, summarized in table 2, are accommodated in the likelihood model as nuisance parameters, the measurements of which are assumed to follow a log-normal distribution. In the case of the modelling of the $H_{\text{T}}^{\text{miss}}$ distribution, alternative templates are used to describe the uncertainties in the modelling and a vertical template morphing schema [29, 92] is used to interpolate between the nominal and alternative templates. The multijet background estimates, determined using the method described in section 6, are also included in the likelihood model.

Figures 1 and 2 summarize the binned counts of signal events and the corresponding SM expectations as determined from a "CR-only" fit that uses only the data counts in the μ+jets and $\mu\mu$+jets control regions to constrain the model parameters related to the nonmultijet backgrounds. The uncertainties in the SM expectations reflect both statistical and systematic components. The multijet background estimates are determined independently and included in the SM expectations. The fit does not consider the event counts in the signal region.

Hypothesis testing with regards to a potential signal contribution is performed by considering a full fit to the event counts in the SR and CRs. No significant deviation is observed between the predictions and data in the SR and CRs, and the data counts appear to be adequately modelled by the SM expectations with no significant kinematical patterns.

Event counts and SM background estimates, and the associated correlation matrix, are also determined using the simplified 32-bin schema, which can be found in table 7 and figure 5 (appendix A), respectively.
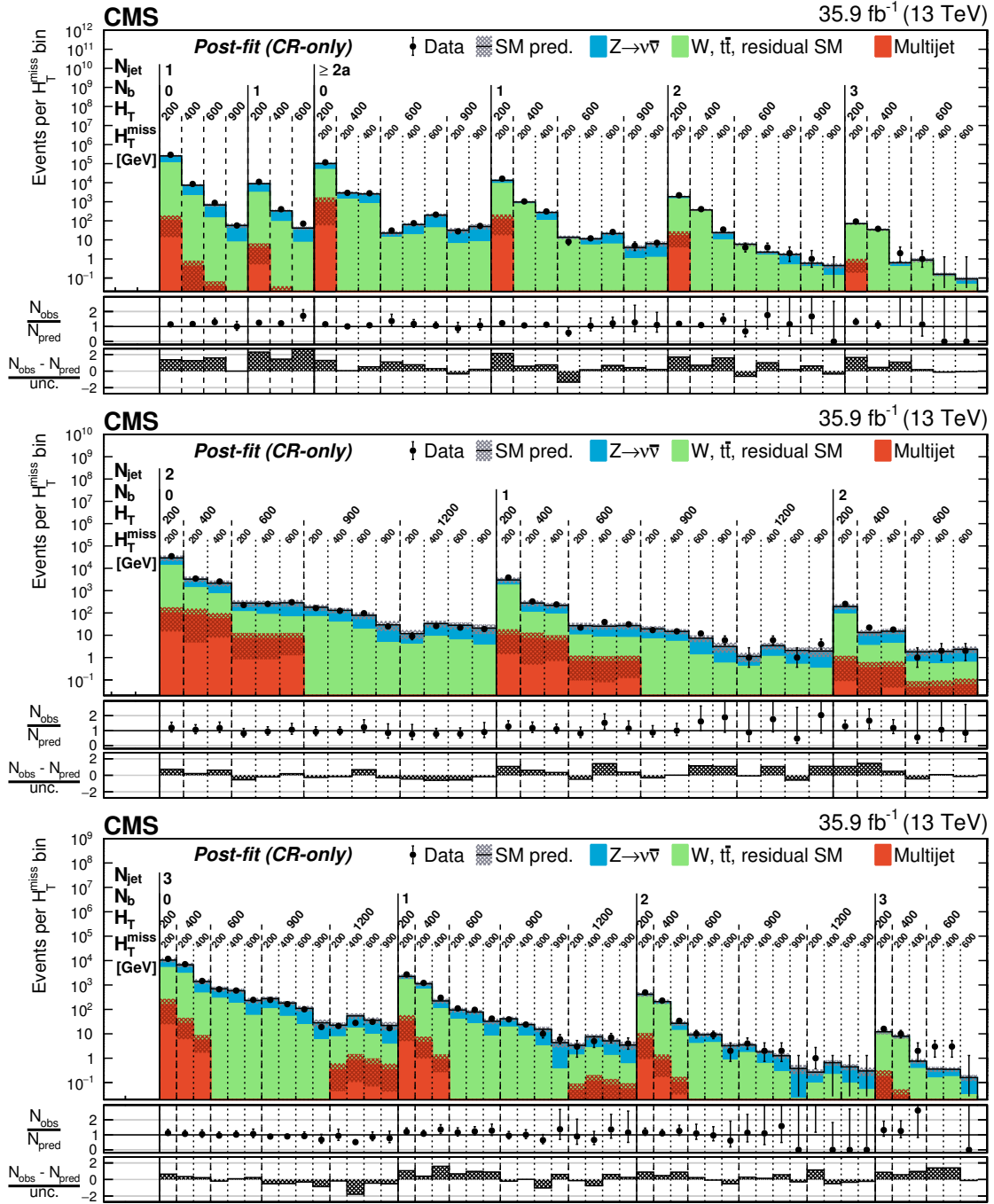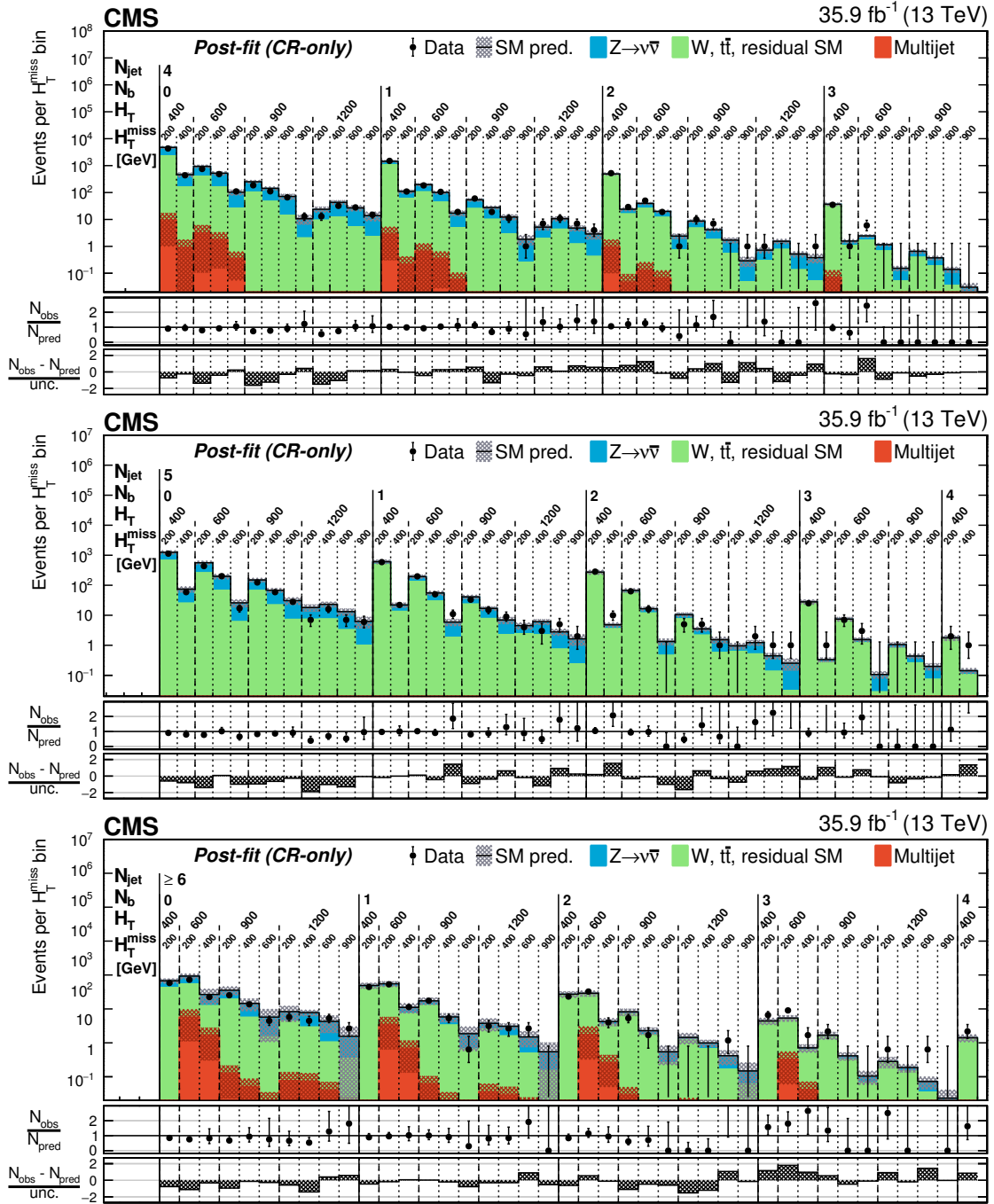
Figure 1. Counts of signal events (solid markers) and SM expectations with associated uncertainties (statistical and systematic, black histograms and shaded bands) as determined from the CR-only fit as a function of n_b, H_T, and H_T^{miss} for the event categories $n_{jet} = 1$ and $\geq 2a$ (upper), $= 2$ (middle), and $= 3$ (lower). The centre panel of each subfigure shows the ratios of observed counts and the SM expectations, while the lower panel shows the significance of deviations observed in data with respect to the SM expectations expressed in terms of the total uncertainty in the SM expectations.

Figure 2. Counts of signal events (solid markers) and SM expectations with associated uncertainties (statistical and systematic, black histograms and shaded bands) as determined from the CR-only fit as a function of n_b, H_T, and H_T^{miss} for the event categories $n_{jet} = 4$ (upper), $= 5$ (middle), and ≥ 6 (lower). The lower panels are described in the caption of figure 1.

Model family	Production and decay	Additional assumptions
Production and prompt decay of squark pairs		
T2bb	$pp \to \widetilde{b}_1\overline{\widetilde{b}}_1,\ \widetilde{b}_1 \to b\widetilde{\chi}_1^0$	—
T2tt	$pp \to \widetilde{t}_1\overline{\widetilde{t}}_1,\ \widetilde{t}_1 \to t\widetilde{\chi}_1^0$	—
T2cc	$pp \to \widetilde{t}_1\overline{\widetilde{t}}_1,\ \widetilde{t}_1 \to c\widetilde{\chi}_1^0$	$10 < m_{\widetilde{t}_1} - m_{\widetilde{\chi}_1^0} < 80\,\mathrm{GeV}$
T2qq_8fold	$pp \to \widetilde{q}\overline{\widetilde{q}},\ \widetilde{q} \to q\widetilde{\chi}_1^0$	$m_{\widetilde{q}_L} = m_{\widetilde{q}_R},\ \widetilde{q} = \{\widetilde{u}, \widetilde{d}, \widetilde{s}, \widetilde{c}\}$
T2qq_1fold	$pp \to \widetilde{q}\overline{\widetilde{q}},\ \widetilde{q} \to q\widetilde{\chi}_1^0$	$m_{\widetilde{q}(\widetilde{q}\neq\widetilde{u}_L)} \gg m_{\widetilde{u}_L}$
Production and prompt decay of gluino pairs		
T1bbbb	$pp \to \widetilde{g}\widetilde{g},\ \widetilde{g} \to \overline{b}\widetilde{b}_1^* \to \overline{b}b\widetilde{\chi}_1^0$	$m_{\widetilde{b}_1} \gg m_{\widetilde{g}}$
T1tttt	$pp \to \widetilde{g}\widetilde{g},\ \widetilde{g} \to \overline{t}\widetilde{t}_1^* \to \overline{t}t\widetilde{\chi}_1^0$	$m_{\widetilde{t}_1} \gg m_{\widetilde{g}}$
T1qqqq	$pp \to \widetilde{g}\widetilde{g},\ \widetilde{g} \to \overline{q}\widetilde{q}^* \to \overline{q}q\widetilde{\chi}_1^0$	$m_{\widetilde{q}} \gg m_{\widetilde{g}}$
Production and decay of long-lived gluino pairs		
T1qqqqLL	$pp \to \widetilde{g}\widetilde{g},\ \widetilde{g} \to \overline{q}\widetilde{q}^* \to \overline{q}q\widetilde{\chi}_1^0$	$m_{\widetilde{q}} \gg m_{\widetilde{g}},\ 10^{-3} < c\tau_0 < 10^5\,\mathrm{mm}$ or metastable

Table 3. Summary of the simplified SUSY models used to interpret the result of this search.

8 Interpretations

The search result is used to constrain the parameter spaces of simplified SUSY models [30–32]. Interpretations are provided for nine unique model families, as summarized in table 3. Each family of models realizes a unique production and decay mode. The model parameters are the masses of the parent gluino ($m_{\widetilde{g}}$) or bottom, top, and LF ($m_{\widetilde{b}_1}$, $m_{\widetilde{t}_1}$, $m_{\widetilde{q}}$) squark, also collectively labelled as m_{SUSY}, and the $\widetilde{\chi}_1^0$ ($m_{\widetilde{\chi}_1^0}$). Two scenarios are considered for LF squarks: one with an eightfold mass degeneracy for $\widetilde{q}_L$ and $\widetilde{q}_R$ with $\widetilde{q} = \{\widetilde{u}, \widetilde{d}, \widetilde{s}, \widetilde{c}\}$ and the other with just a single light squark ($\widetilde{u}_L$). All other SUSY particles are assumed to be too heavy to be produced directly. Gluinos are assumed to undergo prompt three-body decays via highly virtual squarks. In the case of split SUSY models (T1qqqqLL), the gluino is assumed to be long-lived with proper decay lengths in the range $10^{-3} < c\tau_0 < 10^5\,\mathrm{mm}$. A scenario involving a metastable gluino with $c\tau_0 = 10^{18}\,\mathrm{mm}$ is also considered.

Under the signal+background hypothesis, and in the presence of a nonzero signal contribution, a modified frequentist approach is used to determine observed upper limits (ULs) at 95% confidence level (CL) on the cross section σ_{UL} to produce pairs of SUSY particles as a function of m_{SUSY}, $m_{\widetilde{\chi}_1^0}$, and $c\tau_0$ (if applicable). The approach is based on the profile likelihood ratio as the test statistic [93], the $\mathrm{CL_s}$ criterion [94, 95], and the asymptotic formulae [96] to approximate the distributions of the test statistic under the SM-background-only and signal+background hypotheses. An Asimov data set [96] is used to determine the expected σ_{UL} on the allowed cross section for a given model. Potential signal contributions to event counts in all bins of the SR and CRs are considered.

The experimental acceptance times efficiency ($\mathcal{A}\varepsilon$) is evaluated independently for each model, defined in terms of m_{SUSY}, $m_{\widetilde{\chi}_1^0}$, and $c\tau_0$ (if applicable). The effects of several sources of uncertainty in $\mathcal{A}\varepsilon$, as well as the potential for migration of events between bins

of the SR, are considered. Correlations are taken into account where appropriate, including those relevant to signal contamination that may contribute to counts in the CRs.

The statistical uncertainty arising from the finite size of simulated samples can be as large as $\approx 30\%$. The $\mathcal{A}\varepsilon$ for models with a compressed mass spectrum relies on jets arising from ISR, the modelling of which is evaluated using the technique described in ref. [67]. The associated uncertainty can be as large as $\approx 30\%$. The corrections to the jet energy scale (JES) evaluated with simulated events can lead to variations in event counts as large as $\approx 25\%$ for models yielding high jet multiplicities. The uncertainties in the modelling of scale factors applied to simulated event samples that correct for differences in the b tagging efficiency and mistag probabilities can be as large as $\approx 20\%$.

Table 4 defines a number of benchmark models that are close to the limit of the search sensitivity. All model families are represented, and the model parameters (m_{SUSY}, $m_{\widetilde{\chi}_1^0}$, and $c\tau_0$ if applicable) are chosen to select models with large and small differences in m_{SUSY} and $m_{\widetilde{\chi}_1^0}$, as well as a range of $c\tau_0$ values. Table 4 summarizes the aforementioned uncertainties for each benchmark model, presented in terms of a characteristic range that is representative of the variations observed across the bins of the SR. The upper bound for each range may be subject to moderate statistical fluctuations.

Additional subdominant contributions to the total uncertainty are also considered. The uncertainty in the integrated luminosity is determined to be 2.5% [23]. Uncertainties in the production cross section arising from the choice of the PDF set, and variations therein, as well as variations in μ_{F} and μ_{R} at LO are considered. Uncertainties in event migration between bins from variations in the PDF sets are assumed to be correlated with, and adequately covered by, the uncertainties in the modelling of ISR. Uncertainties from μ_{F} and μ_{R} variations are determined to be $\approx 5\%$. The effect of a 5% uncertainty in the total inelastic cross section [91] is propagated through the weighting procedure that corrects for differences between the simulated and measured pileup, resulting in event count variations of $\approx 10\%$. Uncertainty in the modelling of the efficiency to identify high-quality, isolated leptons is $\approx 5\%$ and is treated as anticorrelated between the SR and μ+jets and $\mu\mu$+jets CRs. The uncertainty in the trigger efficiency to record signal events is $< 10\%$.

The $\mathcal{A}\varepsilon$ for the T1qqqqLL family of models depends on $c\tau_0$ in addition to $m_{\widetilde{\mathrm{g}}}$ and $m_{\widetilde{\chi}_1^0}$. Scenarios involving a compressed mass spectrum or gluinos with $c\tau_0 \gtrsim 10\,\mathrm{m}$ increase the probability that the decay of the gluino-pair system escapes detection, and the $\mathcal{A}\varepsilon$ is reduced for such models, as indicated in table 4, because of an increased reliance on jets from ISR. Scenarios with $m_{\widetilde{\mathrm{g}}} - m_{\widetilde{\chi}_1^0} \gtrsim 100\,\mathrm{GeV}$ and $1 \lesssim c\tau_0 \lesssim 10\,\mathrm{m}$ often lead to one or both gluinos decaying within the calorimeter systems to yield energetic jets comprising particle candidates that have no associated charged particle track. Hence, the efficiencies for the event vetoes related to the jet identification and $f_{\mathrm{h}\pm}^{\mathrm{j}1}$ requirements, described in sections 2 and 3.1, can be as low as $\approx 90\%$ and $\approx 30\%$, respectively, for this region of the model parameter space. Uncertainties as large as $\approx 10\%$ are assumed. The efficiencies for all other scenarios are typically $\approx 100\%$. Jet identification requirements in the trigger logic lead to inefficiencies and uncertainties not larger than 2%. Finally, models with $1 \lesssim c\tau_0 \lesssim 10\,\mathrm{mm}$ often lead to jets that are tagged by the CSV algorithm with efficiencies as high as $\approx 60\%$, which are comparable to the values obtained for jets originating from b

Family	$(m_{\mathrm{SUSY}}, m_{\widetilde{\chi}_1^0})$	$\mathcal{A}\varepsilon$	Systematic uncertainties [%]				$\sigma_{\mathrm{UL}}/\sigma_{\mathrm{th}}$ (95% CL)	
$(c\tau_0)$	[GeV]	[%]	MC stat.	ISR	JES	b tagging	Exp.	Obs.
T2bb	(1000, 100)	40.1	14–23	1–7	4–11	1–4	0.62	0.67
	(550, 450)	5.7	9–22	4–15	4–15	3–7	0.76	1.21
	(1000, 50)	23.8	14–27	3–7	4–14	1–5	0.82	0.85
T2tt	(450, 200)	4.2	6–19	4–12	6–15	4–9	0.56	0.73
	(250, 150)	0.3	10–23	13–27	8–22	6–16	0.71	0.66
T2cc	(500, 480)	20.5	6–19	4–18	5–13	1–4	0.68	1.38
T2qq_8fold	(1250, 100)	42.9	12–24	2–7	5–14	1–1	0.54	0.66
	(700, 600)	7.7	6–22	4–17	4–13	2–5	0.75	1.13
T2qq_1fold	(700, 100)	32.9	4–22	2–7	3–10	0–5	0.60	0.88
	(400, 300)	4.5	6–20	5–22	5–18	3–5	0.61	0.46
T1bbbb	(1900, 100)	25.1	11–19	3–9	4–6	7–11	0.56	1.25
	(1300, 1100)	14.6	11–22	2–11	3–11	2–5	0.44	1.15
T1tttt	(1700, 100)	6.9	12–24	2–6	3–15	2–6	0.51	1.31
	(950, 600)	0.3	15–30	5–9	12–26	2–6	0.89	1.51
T1qqqqLL	(1800, 200)	27.8	8–20	3–5	3–9	0–1	1.02	1.91
$(1\,\mu\mathrm{m})$	(1000, 900)	6.7	15–21	2–10	4–14	0–1	0.68	1.26
T1qqqqLL	(1800, 200)	22.9	11–20	2–5	3–9	17–59	0.43	1.00
$(1\,\mathrm{mm})$	(1000, 900)	5.2	17–26	2–9	4–17	10–41	0.28	0.63
T1qqqqLL	(1000, 200)	11.2	16–22	2–14	4–9	0–1	0.74	1.58
$(100\,\mathrm{m})$	(1000, 900)	10.4	14–26	3–14	2–12	0–1	0.63	0.45

Table 4. A list of benchmark simplified models organized according to production and decay modes (family), the $\mathcal{A}\varepsilon$, representative values for some of the dominant sources of systematic uncertainty, and the expected and observed upper limits on the production cross section σ_{UL} relative to the theoretical value σ_{th} calculated at NLO+NLL accuracy. Additional uncertainties concerning the T1qqqqLL models are not listed here and are discussed in the text.

quarks. Uncertainties of 20–50% in the tagging efficiency are assumed to cover differences with respect to jets originating from b quarks, as indicated in table 4.

Figure 3 summarizes the excluded regions of the mass parameter space for the nine families of simplified models. The regions are determined by comparing σ_{UL} with the theoretical cross sections σ_{th} calculated at NLO+NLL accuracy. The former value is determined as a function of m_{SUSY} and $m_{\widetilde{\chi}_1^0}$, while the latter has a dependence solely on m_{SUSY}. The exclusion of models is evaluated using observed data counts in the signal region (solid contours) and also expected counts based on an Asimov data set (dashed contours). The observed excluded regions for the T1bbbb and T1tttt families, as shown in figure 3 (lower), can be up to 2–3 standard deviations weaker than the expected excluded regions when $m_{\widetilde{g}} - m_{\widetilde{\chi}_1^0} \approx 350\,\mathrm{GeV}$. These differences are typically due to fluctuations in data for events that satisfy $n_{\mathrm{jet}} \geq 5$ and $n_{\mathrm{b}} \geq 3$. Figure 3 (lower) also allows a comparison of the sensitivity
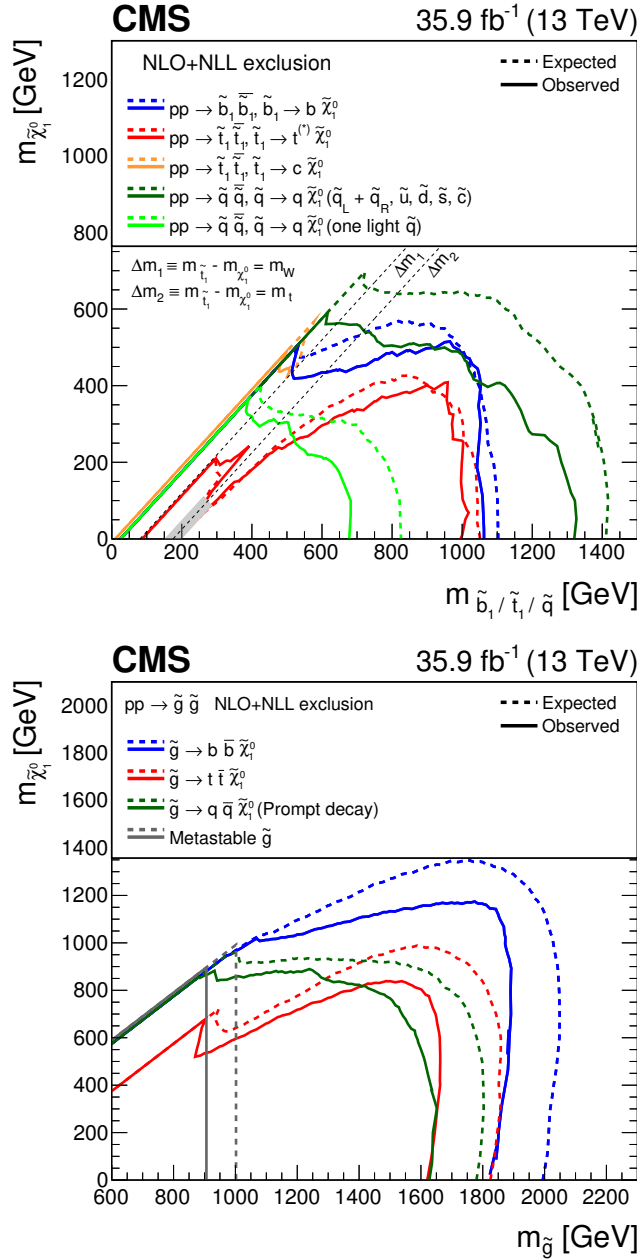
Figure 3. Observed and expected mass exclusions at 95% CL (indicated, respectively, by solid and dashed contours) for various families of simplified models. The upper subfigure summarises the mass exclusions for five model families that involve the direct pair production of squarks. The first scenario considers the pair production and decay of bottom squarks (T2bb). Two scenarios involve the production and decay of top squark pairs (T2tt and T2cc). The grey shaded region denotes T2tt models that are not considered for interpretation. Two further scenarios involve, respectively, the production and decay of light-flavour squarks, with different assumptions on the mass degeneracy of the squarks as described in the text (T2qq_8fold and T2qq_1fold). The lower subfigure summarises three scenarios that involve the production and prompt decay of gluino pairs via virtual squarks (T1bbbb, T1tttt, and T1qqqq). A final scenario involves the production of gluinos that are assumed to be metastable on the detector scale (T1qqqqLL).
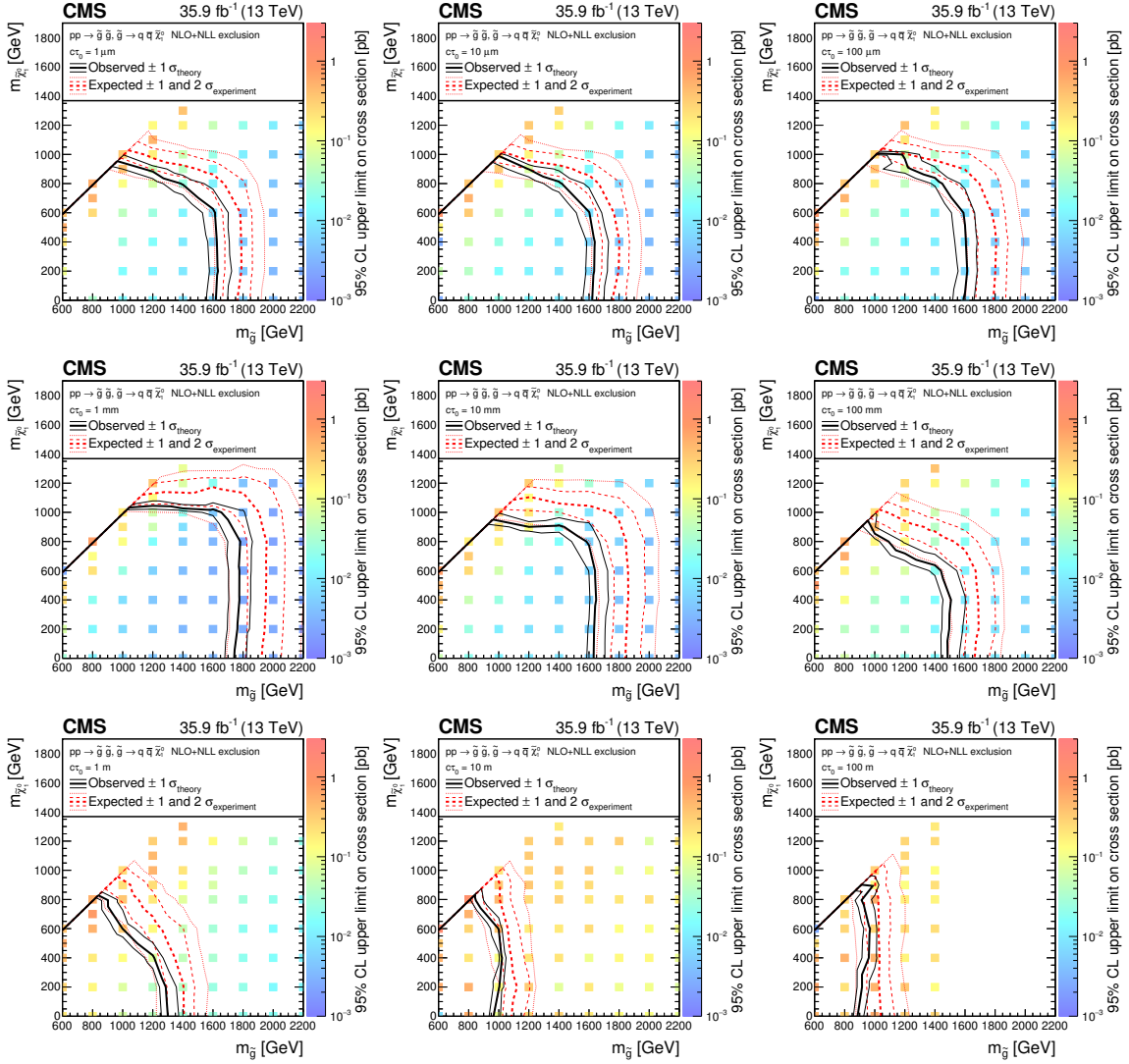
Figure 4. Observed upper limit in cross section at 95% CL (indicated by the colour scale) as a function of the $\widetilde{g}$ and $\widetilde{\chi}_1^0$ masses for simplified models that assume the production of pairs of long-lived gluinos that each decay via highly virtual light-flavour squarks to the neutralino and SM particles (T1qqqqLL). Each subfigure represents a different gluino lifetime: $c\tau_0 = 1$ (upper left), 10 (upper centre), and 100 μm (upper right); 1 (middle left), 10 (middle centre), and 100 mm (middle right); and 1 (lower left), 10 (lower centre), and 100 m (lower right). The thick (thin) black solid line indicates the observed excluded region assuming the nominal (± 1 standard deviation in theoretical uncertainty) production cross section. The red thick dashed (thin dashed and dotted) line indicates the median (± 1 and 2 standard deviations in experimental uncertainty) expected excluded region.

to T1qqqq and T1qqqqLL models, which assume the prompt-decay and metastable gluino scenarios, respectively. The latter scenario leads to a monojet-like final state as the gluino escapes detection, resulting in a reach in $m_{\widetilde{g}}$ that is independent of $m_{\widetilde{\chi}_1^0}$.

Figure 4 summarizes the evolution of the search sensitivity to the T1qqqqLL family of models as a function of $c\tau_0$. Each subfigure presents the observed σ_{UL} as a function of $m_{\widetilde{g}}$

Model family	Best mass limit [GeV]	
	Gluino or squark	$\widetilde{\chi}_1^0$
T2bb	1050	500
T2tt	1000	400
T2cc	500	475
T2qq_8fold	1325	575
T2qq_1fold	675	350
T1bbbb	1900	1150
T1tttt	1650	850
T1qqqq	1650	900
T1qqqqLL (Metastable $\widetilde{g}$)	900	—
T1qqqqLL ($c\tau_0 = 1\,\text{mm}$)	1750	1000

Table 5. Summary of the mass limits obtained for each family of simplified models. The limits indicate the strongest observed mass exclusions for the parent SUSY particle (gluino or squark) and $\widetilde{\chi}_1^0$.

and $m_{\widetilde{\chi}_1^0}$ for simplified models that involve the production of gluino pairs. The excluded mass regions based on the observed and expected values of σ_{UL} are also shown, along with contours determined under variations in theoretical and experimental uncertainties. The top row of subfigures cover the range $1 < c\tau_0 < 100\,\mu\text{m}$ and demonstrate coverage comparable to the T1qqqq prompt-decay scenario. A moderate improvement in sensitivity for models with $1 \lesssim c\tau_0 \lesssim 10\,\text{mm}$ is observed because of the additional signal-to-background discrimination provided by the n_{b} variable. The sensitivity is reduced for models with lifetimes in the region $c\tau_0 > 100\,\text{mm}$ because of a lower acceptance for the jets from the gluino decay and an increased reliance on jets from ISR. The coverage is independent of $c\tau_0$ beyond values of $10\,\text{m}$ and comparable to the limiting case of a metastable gluino.

A nonnegligible fraction of R-hadrons that traverse the muon chambers before decaying are identified as muons by the PF algorithm. The fraction is dependent on the R-hadron model and the choice of parameters that affect the hadronization model and matter interactions. The signal $\mathcal{A}\varepsilon$ is strongly dependent on $c\tau_0$ due to the muon veto employed by this search. Under these assumptions, the excluded mass regions shown in figure 4 weaken by 50–200 GeV for models with $c\tau_0 \gtrsim 1\,\text{m}$, with the largest change occurring at $c\tau_0 \approx 10\,\text{m}$. The change is negligible for models with $c\tau_0$ below $1\,\text{m}$.

Table 5 summarizes the strongest expected and observed mass limits for each family of models. The simplified result based on the 32-bin schema, summarized in appendix A, yields limits on σ_{UL} that are typically a factor ≈ 2 weaker than those obtained with the nominal result.

9 Summary

A search for supersymmetry with the CMS experiment is reported, based on a data sample of pp collisions collected in 2016 at $\sqrt{s} = 13\,\text{TeV}$ that corresponds to an integrated luminosity of $35.9 \pm 0.9\,\text{fb}^{-1}$. Final states with jets and significant missing transverse momentum $\vec{p}_\text{T}^{\,\text{miss}}$, as expected from the production and decay of massive gluinos and squarks, are considered. Signal events are categorized according to the number of reconstructed jets, the number of jets identified as originating from bottom quarks, and the scalar and vector sums of the transverse momenta of jets. The standard model background is estimated from a binned likelihood fit to event yields in the signal region and data control samples. The observed yields in the signal region are found to be in agreement with the expected contributions from standard model processes. Supplemental material is provided to aid further interpretation of the result in appendix A.

Limits are determined in the parameter spaces of simplified models that assume the production and prompt decay of gluino or squark pairs. The strongest exclusion bounds (95% confidence level) for squark masses are 1050, 1000, and 1325 GeV for bottom, top, and mass-degenerate light-flavour squarks, respectively. The corresponding mass bounds on the neutralino $\widetilde{\chi}_1^0$ from squark decays are 500, 400, and 575 GeV. The gluino mass is probed up to 1900, 1650, and 1650 GeV when the gluino decays via virtual states of the aforementioned squarks. The strongest mass bound on the $\widetilde{\chi}_1^0$ from the gluino decay is 1150 GeV.

Sensitivity to simplified models inspired by split supersymmetry is also demonstrated. These models assume the production of long-lived gluino pairs that decay to final states containing displaced jets and $\vec{p}_\text{T}^{\,\text{miss}}$ from the undetected $\widetilde{\chi}_1^0$ particles. The long-lived gluino, with an assumed proper decay length $c\tau_0$, is expected to hadronize with SM particles and form a bound state known as an R-hadron. The model-dependent matter interactions of R-hadrons are not considered by default. The sensitivity of this search is only moderately dependent on these matter interactions for models with $c\tau_0 \gtrsim 1\,\text{m}$, while no dependence is found for models with $c\tau_0$ below $1\,\text{m}$. Models that assume a $\widetilde{\chi}_1^0$ mass of $100\,\text{GeV}$ and gluino masses up to $1600\,\text{GeV}$ are excluded for a proper decay length $c\tau_0$ below $0.1\,\text{mm}$. The bound on the gluino mass strengthens to $1750\,\text{GeV}$ at $c\tau_0 = 1\,\text{mm}$, before weakening to 900–$1000\,\text{GeV}$ for models with $c\tau_0 > 10\,\text{m}$. For all values of $c\tau_0$ considered, the exclusion bounds on the gluino mass weaken to about $1\,\text{TeV}$ when the difference between the gluino and $\widetilde{\chi}_1^0$ mass is small. The search provides coverage of the $c\tau_0$ parameter space for models involving long-lived gluinos, such as the region $c\tau_0 \lesssim 1\,\text{mm}$, that is complementary to the coverage provided by dedicated techniques at the LHC.

A Supplemental material

n_{jet}	n_{b}	H_{T} [GeV]
		200	400	600	900	1200
1	0	200	400	600	900	—
1	1	200	400	600	—	—
$\geq 2a$	0	200	200, 400	200, 400, 600	200, 900	—
$\geq 2a$	1	200	200, 400	200, 400, 600	200, 900	—
$\geq 2a$	2	200	200, 400	200, 400, 600	200, 900	—
$\geq 2a$	≥ 3	200	200, 400	200, 400, 600	—	—
2	0	200	200, 400	200, 400, 600	200, 400, 600, 900	200, 400, 600, 900
2	1	200	200, 400	200, 400, 600	200, 400, 600, 900	200, 400, 600, 900
2	2	200	200, 400	200, 400, 600	—	—
3	0	200	200, 400	200, 400, 600	200, 400, 600, 900	200, 400, 600, 900
3	1	200	200, 400	200, 400, 600	200, 400, 600, 900	200, 400, 600, 900
3	2	200	200, 400	200, 400, 600	200, 400, 600, 900	200, 400, 600, 900
3	3	200	200, 400	200, 400, 600	—	—
4	0	—	200, 400	200, 400, 600	200, 400, 600, 900	200, 400, 600, 900
4	1	—	200, 400	200, 400, 600	200, 400, 600, 900	200, 400, 600, 900
4	2	—	200, 400	200, 400, 600	200, 400, 600, 900	200, 400, 600, 900
4	≥ 3	—	200, 400	200, 400, 600	200, 400, 600, 900	—
5	0	—	200, 400	200, 400, 600	200, 400, 600	200, 400, 600, 900
5	1	—	200, 400	200, 400, 600	200, 400, 600	200, 400, 600, 900
5	2	—	200, 400	200, 400, 600	200, 400, 600	200, 400, 600, 900
5	3	—	200, 400	200, 400, 600	200, 400, 600	—
5	≥ 4	—	200, 400	—	—	—
≥ 6	0	—	200	200, 400	200, 400, 600	200, 400, 600, 900
≥ 6	1	—	200	200, 400	200, 400, 600	200, 400, 600, 900
≥ 6	2	—	200	200, 400	200, 400, 600	200, 400, 600, 900
≥ 6	3	—	200	200, 400	200, 400, 600	200, 400, 600, 900
≥ 6	≥ 4	—	200	—	—	—

Table 6. Summary of the nominal (n_{jet}, n_{b}, H_{T}, $H_{\mathrm{T}}^{\mathrm{miss}}$) binning schema. Each entry (and the following entry, if present) signifies the lower (upper) bound of an $H_{\mathrm{T}}^{\mathrm{miss}}$ bin within a given (n_{jet}, n_{b}, H_{T}) bin. Unique or final entries represent $H_{\mathrm{T}}^{\mathrm{miss}}$ bins unbounded from above. A dash (—) signifies that the H_{T} bin in a given (n_{jet}, n_{b}) category is not used in the analysis, in which case counts in high-H_{T} bins are integrated into the adjacent lower-H_{T} bin. For monojet events, $H_{\mathrm{T}} \equiv H_{\mathrm{T}}^{\mathrm{miss}}$. The a denotes asymmetric p_{T} thresholds for the two highest p_{T} jets.

n_{jet}	n_{b}		$H_{\text{T}}^{\text{miss}}$ [GeV]			
			200	400	600	900
$=1, \geq 2a$	0	Data	411 184	11 448	1116	111
		SM	$360\,000 \pm 38\,000$	$10\,000 \pm 1400$	910 ± 170	107 ± 28
$=1, \geq 2a$	≥ 1	Data	31 174	769	105	7
		SM	$25\,500 \pm 2500$	649 ± 91	69 ± 13	6.4 ± 1.8
$=2, =3$	$=0, =1$	Data	66 955	5946	903	100
		SM	$58\,000 \pm 11\,000$	5400 ± 1100	860 ± 220	113 ± 41
$=2, =3$	≥ 2	Data	1045	70	6	0
		SM	870 ± 130	56.9 ± 9.4	7.1 ± 1.7	1.0 ± 0.4
$=4, =5$	$=0, =1$	Data	9546	1734	315	44
		SM	$10\,500 \pm 1100$	1880 ± 310	319 ± 71	40 ± 14
$=4, =5$	≥ 2	Data	1012	93	4	3
		SM	970 ± 110	81 ± 11	8.4 ± 1.7	1.2 ± 0.4
≥ 6	$=0, =1$	Data	758	141	33	5
		SM	910 ± 180	167 ± 76	33 ± 25	4.2 ± 5.0
≥ 6	≥ 2	Data	197	14	3	0
		SM	189 ± 40	16.9 ± 4.9	2.1 ± 1.2	0.2 ± 0.2

Table 7. Observed counts of candidate signal events and SM expectations determined from the CR-only fit using the simplified binning schema, as a function of n_{jet}, n_{b}, and $H_{\text{T}}^{\text{miss}}$. All counts are integrated over H_{T}. The uncertainties include both statistical and systematic contributions. The a denotes asymmetric p_{T} thresholds for the two highest p_{T} jets.
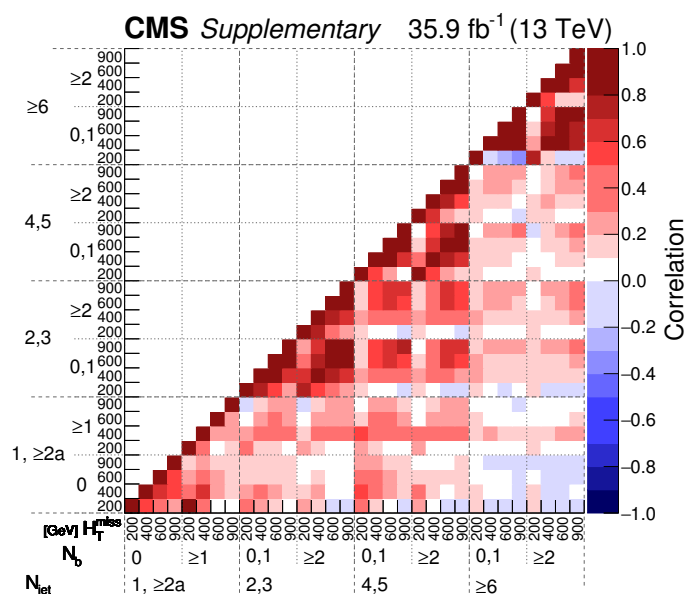

Figure 5. Correlation matrix for the SM background estimates determined from the CR-only fit using the simplified binning schema defined in table 7.

References

[1] Yu.A. Golfand and E.P. Likhtman, *Extension of the Algebra of Poincaré Group Generators and Violation of p Invariance*, *JETP Lett.* **13** (1971) 323 [ɪɴSPIRE].

[2] J. Wess and B. Zumino, *Supergauge Transformations in Four-Dimensions*, *Nucl. Phys.* **B 70** (1974) 39 [ɪɴSPIRE].

[3] R. Barbieri, S. Ferrara and C.A. Savoy, *Gauge Models with Spontaneously Broken Local Supersymmetry*, *Phys. Lett.* **B 119** (1982) 343 [ɪɴSPIRE].

[4] H.P. Nilles, *Supersymmetry, Supergravity and Particle Physics*, *Phys. Rept.* **110** (1984) 1 [ɪɴSPIRE].

[5] E. Witten, *Dynamical Breaking of Supersymmetry*, *Nucl. Phys.* **B 188** (1981) 513 [ɪɴSPIRE].

[6] S. Dimopoulos and H. Georgi, *Softly Broken Supersymmetry and* SU(5), *Nucl. Phys.* **B 193** (1981) 150 [ɪɴSPIRE].

[7] S. Dimopoulos, S. Raby and F. Wilczek, *Supersymmetry and the Scale of Unification*, *Phys. Rev.* **D 24** (1981) 1681 [ɪɴSPIRE].

[8] L.E. Ibáñez and G.G. Ross, *Low-Energy Predictions in Supersymmetric Grand Unified Theories*, *Phys. Lett.* **B 105** (1981) 439 [ɪɴSPIRE].

[9] W.J. Marciano and G. Senjanović, *Predictions of Supersymmetric Grand Unified Theories*, *Phys. Rev.* **D 25** (1982) 3092 [ɪɴSPIRE].

[10] G.R. Farrar and P. Fayet, *Phenomenology of the Production, Decay and Detection of New Hadronic States Associated with Supersymmetry*, *Phys. Lett.* **B 76** (1978) 575 [ɪɴSPIRE].

[11] G. Jungman, M. Kamionkowski and K. Griest, *Supersymmetric dark matter*, *Phys. Rept.* **267** (1996) 195 [hep-ph/9506380] [ɪɴSPIRE].

[12] PARTICLE DATA GROUP collaboration, C. Patrignani et al., *Review of Particle Physics*, *Chin. Phys.* **C 40** (2016) 100001 [ɪɴSPIRE].

[13] R. Barbieri and D. Pappadopulo, *S-particles at their naturalness limits*, *JHEP* **10** (2009) 061 [arXiv:0906.4546] [ɪɴSPIRE].

[14] ATLAS collaboration, *Observation of a new particle in the search for the Standard Model Higgs boson with the ATLAS detector at the LHC*, *Phys. Lett.* **B 716** (2012) 1 [arXiv:1207.7214] [ɪɴSPIRE].

[15] CMS collaboration, *Observation of a new boson at a mass of 125 GeV with the CMS experiment at the LHC*, *Phys. Lett.* **B 716** (2012) 30 [arXiv:1207.7235] [ɪɴSPIRE].

[16] CMS collaboration, *Observation of a new boson with mass near 125 GeV in pp collisions at $\sqrt{s} = 7$ and 8 TeV*, *JHEP* **06** (2013) 081 [arXiv:1303.4571] [ɪɴSPIRE].

[17] CMS collaboration, *Precise determination of the mass of the Higgs boson and tests of compatibility of its couplings with the standard model predictions using proton collisions at 7 and 8 TeV*, *Eur. Phys. J.* **C 75** (2015) 212 [arXiv:1412.8662] [ɪɴSPIRE].

[18] ATLAS collaboration, *Measurement of the Higgs boson mass from the $H \to \gamma\gamma$ and $H \to ZZ^* \to 4\ell$ channels with the ATLAS detector using 25 fb^{-1} of pp collision data*, *Phys. Rev.* **D 90** (2014) 052004 [arXiv:1406.3827] [ɪɴSPIRE].

[19] ATLAS, CMS collaboration, *Combined Measurement of the Higgs Boson Mass in pp Collisions at $\sqrt{s} = 7$ and 8 TeV with the ATLAS and CMS Experiments*, *Phys. Rev. Lett.* **114** (2015) 191803 [arXiv:1503.07589] [InSPIRE].

[20] N. Arkani-Hamed and S. Dimopoulos, *Supersymmetric unification without low energy supersymmetry and signatures for fine-tuning at the LHC*, *JHEP* **06** (2005) 073 [hep-th/0405159] [InSPIRE].

[21] G.F. Giudice and A. Romanino, *Split supersymmetry*, *Nucl. Phys.* **B 699** (2004) 65 [*Erratum ibid.* **B 706** (2005) 487] [hep-ph/0406088] [InSPIRE].

[22] M. Fairbairn, A.C. Kraan, D.A. Milstead, T. Sjöstrand, P.Z. Skands and T. Sloan, *Stable massive particles at colliders*, *Phys. Rept.* **438** (2007) 1 [hep-ph/0611040] [InSPIRE].

[23] CMS collaboration, *CMS Luminosity Measurements for the 2016 Data Taking Period*, CMS-PAS-LUM-17-001 (2017).

[24] CMS collaboration, *Search for Supersymmetry in pp Collisions at 7 TeV in Events with Jets and Missing Transverse Energy*, *Phys. Lett.* **B 698** (2011) 196 [arXiv:1101.1628] [InSPIRE].

[25] CMS collaboration, *Search for Supersymmetry at the LHC in Events with Jets and Missing Transverse Energy*, *Phys. Rev. Lett.* **107** (2011) 221804 [arXiv:1109.2352] [InSPIRE].

[26] CMS collaboration, *Search for supersymmetry in final states with missing transverse energy and $0, 1, 2$, or ≥ 3 b-quark jets in 7 TeV pp collisions using the variable $\alpha_{\rm T}$*, *JHEP* **01** (2013) 077 [arXiv:1210.8115] [InSPIRE].

[27] CMS collaboration, *Search for supersymmetry in hadronic final states with missing transverse energy using the variables α_T and b-quark multiplicity in pp collisions at $\sqrt{s} = 8$ TeV*, *Eur. Phys. J.* **C 73** (2013) 2568 [arXiv:1303.2985] [InSPIRE].

[28] CMS collaboration, *Search for top squark pair production in compressed-mass-spectrum scenarios in proton-proton collisions at $\sqrt{s} = 8$ TeV using the α_T variable*, *Phys. Lett.* **B 767** (2017) 403 [arXiv:1605.08993] [InSPIRE].

[29] CMS collaboration, *A search for new phenomena in pp collisions at $\sqrt{s} = 13$ TeV in final states with missing transverse momentum and at least one jet using the $\alpha_{\rm T}$ variable*, *Eur. Phys. J.* **C 77** (2017) 294 [arXiv:1611.00338] [InSPIRE].

[30] J. Alwall, P. Schuster and N. Toro, *Simplified Models for a First Characterization of New Physics at the LHC*, *Phys. Rev.* **D 79** (2009) 075020 [arXiv:0810.3921] [InSPIRE].

[31] J. Alwall, M.-P. Le, M. Lisanti and J.G. Wacker, *Model-Independent Jets plus Missing Energy Searches*, *Phys. Rev.* **D 79** (2009) 015005 [arXiv:0809.3264] [InSPIRE].

[32] LHC New Physics Working Group collaboration, D. Alves, *Simplified Models for LHC New Physics Searches*, *J. Phys.* **G 39** (2012) 105005 [arXiv:1105.2838] [InSPIRE].

[33] ATLAS collaboration, *Search for squarks and gluinos in final states with jets and missing transverse momentum at $\sqrt{s} = 13$ TeV with the ATLAS detector*, *Eur. Phys. J.* **C 76** (2016) 392 [arXiv:1605.03814] [InSPIRE].

[34] CMS collaboration, *Search for supersymmetry in multijet events with missing transverse momentum in proton-proton collisions at 13 TeV*, *Phys. Rev.* **D 96** (2017) 032003 [arXiv:1704.07781] [InSPIRE].

[35] CMS collaboration, *Search for new phenomena with the $M_{\rm T2}$ variable in the all-hadronic final state produced in proton-proton collisions at $\sqrt{s} = 13$ TeV*, *Eur. Phys. J.* **C 77** (2017) 710 [arXiv:1705.04650] [InSPIRE].

[36] CMS collaboration, *Search for Stopped Gluinos in pp collisions at $\sqrt{s} = 7\,TeV$*, *Phys. Rev. Lett.* **106** (2011) 011801 [arXiv:1011.5861] [InSPIRE].

[37] CMS collaboration, *Search for Heavy Stable Charged Particles in pp collisions at $\sqrt{s} = 7\,TeV$*, *JHEP* **03** (2011) 024 [arXiv:1101.1645] [InSPIRE].

[38] ATLAS collaboration, *Search for stable hadronising squarks and gluinos with the ATLAS experiment at the LHC*, *Phys. Lett.* **B 701** (2011) 1 [arXiv:1103.1984] [InSPIRE].

[39] ATLAS collaboration, *Search for decays of stopped, long-lived particles from $7\,TeV$ pp collisions with the ATLAS detector*, *Eur. Phys. J.* **C 72** (2012) 1965 [arXiv:1201.5595] [InSPIRE].

[40] CMS collaboration, *Search for heavy long-lived charged particles in pp collisions at $\sqrt{s} = 7\,TeV$*, *Phys. Lett.* **B 713** (2012) 408 [arXiv:1205.0272] [InSPIRE].

[41] ATLAS collaboration, *Search for long-lived stopped R-hadrons decaying out-of-time with pp collisions using the ATLAS detector*, *Phys. Rev.* **D 88** (2013) 112003 [arXiv:1310.6584] [InSPIRE].

[42] CMS collaboration, *Search for Decays of Stopped Long-Lived Particles Produced in Proton-Proton Collisions at $\sqrt{s} = 8\,TeV$*, *Eur. Phys. J.* **C 75** (2015) 151 [arXiv:1501.05603] [InSPIRE].

[43] ATLAS collaboration, *Search for massive, long-lived particles using multitrack displaced vertices or displaced lepton pairs in pp collisions at $\sqrt{s} = 8\,TeV$ with the ATLAS detector*, *Phys. Rev.* **D 92** (2015) 072004 [arXiv:1504.05162] [InSPIRE].

[44] ATLAS collaboration, *Search for metastable heavy charged particles with large ionization energy loss in pp collisions at $\sqrt{s} = 13\,TeV$ using the ATLAS experiment*, *Phys. Rev.* **D 93** (2016) 112015 [arXiv:1604.04520] [InSPIRE].

[45] CMS collaboration, *Search for long-lived charged particles in proton-proton collisions at $\sqrt{s} = 13\,TeV$*, *Phys. Rev.* **D 94** (2016) 112004 [arXiv:1609.08382] [InSPIRE].

[46] ATLAS collaboration, *Search for long-lived, massive particles in events with displaced vertices and missing transverse momentum in $\sqrt{s} = 13\,TeV$ pp collisions with the ATLAS detector*, *Phys. Rev.* **D 97** (2018) 052012 [arXiv:1710.04901] [InSPIRE].

[47] CMS collaboration, *The CMS Experiment at the CERN LHC*, 2008 *JINST* **3** S08004 [InSPIRE].

[48] CMS collaboration, *The CMS trigger system*, 2017 *JINST* **12** P01020 [arXiv:1609.02366] [InSPIRE].

[49] CMS collaboration, *Particle-flow reconstruction and global event description with the CMS detector*, 2017 *JINST* **12** P10003 [arXiv:1706.04965] [InSPIRE].

[50] CMS collaboration, *Performance of Photon Reconstruction and Identification with the CMS Detector in Proton-Proton Collisions at $\sqrt{s} = 8\,TeV$*, 2015 *JINST* **10** P08010 [arXiv:1502.02702] [InSPIRE].

[51] CMS collaboration, *Performance of Electron Reconstruction and Selection with the CMS Detector in Proton-Proton Collisions at $\sqrt{s} = 8\,TeV$*, 2015 *JINST* **10** P06005 [arXiv:1502.02701] [InSPIRE].

[52] CMS collaboration, *Performance of CMS muon reconstruction in pp collision events at $\sqrt{s} = 7\,TeV$*, 2012 *JINST* **7** P10002 [arXiv:1206.4071] [InSPIRE].

[53] M. Cacciari, G.P. Salam and G. Soyez, *The anti-k_T jet clustering algorithm*, *JHEP* **04** (2008) 063 [arXiv:0802.1189] [InSPIRE].

[54] M. Cacciari, G.P. Salam and G. Soyez, *FastJet User Manual*, *Eur. Phys. J.* **C 72** (2012) 1896 [arXiv:1111.6097] [INSPIRE].

[55] M. Cacciari and G.P. Salam, *Pileup subtraction using jet areas*, *Phys. Lett.* **B 659** (2008) 119 [arXiv:0707.1378] [INSPIRE].

[56] K. Rehermann and B. Tweedie, *Efficient Identification of Boosted Semileptonic Top Quarks at the LHC*, *JHEP* **03** (2011) 059 [arXiv:1007.2221] [INSPIRE].

[57] CMS collaboration, *Study of pileup removal algorithms for jets*, CMS-PAS-JME-14-001 (2014).

[58] CMS collaboration, *Jet energy scale and resolution in the CMS experiment in pp collisions at 8 TeV*, 2017 *JINST* **12** P02014 [arXiv:1607.03663] [INSPIRE].

[59] CMS collaboration, *Determination of Jet Energy Calibration and Transverse Momentum Resolution in CMS*, 2011 *JINST* **6** P11002 [arXiv:1107.4277] [INSPIRE].

[60] CMS collaboration, *Identification of heavy-flavour jets with the CMS detector in pp collisions at 13 TeV*, submitted to *JINST* (2017) [arXiv:1712.07158] [INSPIRE].

[61] CMS collaboration, *Performance of missing energy reconstruction in 13 TeV pp collision data using the CMS detector*, CMS-PAS-JME-16-004 (2016).

[62] CMS collaboration, *Performance of the CMS missing transverse momentum reconstruction in pp data at $\sqrt{s} = 8$ TeV*, 2015 *JINST* **10** P02006 [arXiv:1411.0511] [INSPIRE].

[63] L. Randall and D. Tucker-Smith, *Dijet Searches for Supersymmetry at the LHC*, *Phys. Rev. Lett.* **101** (2008) 221803 [arXiv:0806.1049] [INSPIRE].

[64] J. Alwall et al., *The automated computation of tree-level and next-to-leading order differential cross sections and their matching to parton shower simulations*, *JHEP* **07** (2014) 079 [arXiv:1405.0301] [INSPIRE].

[65] J.H. Kuhn, A. Kulesza, S. Pozzorini and M. Schulze, *Electroweak corrections to hadronic photon production at large transverse momenta*, *JHEP* **03** (2006) 059 [hep-ph/0508253] [INSPIRE].

[66] CMS collaboration, *Search for dark matter in proton-proton collisions at 8 TeV with missing transverse momentum and vector boson tagged jets*, *JHEP* **12** (2016) 083 [*Erratum ibid.* **08** (2017) 035] [arXiv:1607.05764] [INSPIRE].

[67] CMS collaboration, *Search for top-squark pair production in the single-lepton final state in pp collisions at $\sqrt{s} = 8$ TeV*, *Eur. Phys. J.* **C 73** (2013) 2677 [arXiv:1308.1586] [INSPIRE].

[68] S. Alioli, P. Nason, C. Oleari and E. Re, *A general framework for implementing NLO calculations in shower Monte Carlo programs: the POWHEG BOX*, *JHEP* **06** (2010) 043 [arXiv:1002.2581] [INSPIRE].

[69] E. Re, *Single-top Wt-channel production matched with parton showers using the POWHEG method*, *Eur. Phys. J.* **C 71** (2011) 1547 [arXiv:1009.2450] [INSPIRE].

[70] T. Sjöstrand et al., *An Introduction to PYTHIA 8.2*, *Comput. Phys. Commun.* **191** (2015) 159 [arXiv:1410.3012] [INSPIRE].

[71] NNPDF collaboration, R.D. Ball et al., *Parton distributions for the LHC Run II*, *JHEP* **04** (2015) 040 [arXiv:1410.8849] [INSPIRE].

[72] R. Gavin, Y. Li, F. Petriello and S. Quackenbush, *W Physics at the LHC with FEWZ 2.1*, *Comput. Phys. Commun.* **184** (2013) 208 [arXiv:1201.5896] [INSPIRE].

[73] R. Gavin, Y. Li, F. Petriello and S. Quackenbush, *FEWZ 2.0: A code for hadronic Z production at next-to-next-to-leading order*, *Comput. Phys. Commun.* **182** (2011) 2388 [arXiv:1011.3540] [INSPIRE].

[74] T. Melia, P. Nason, R. Rontsch and G. Zanderighi, *W^+W^-, WZ and ZZ production in the POWHEG BOX*, *JHEP* **11** (2011) 078 [arXiv:1107.5051] [INSPIRE].

[75] M. Czakon and A. Mitov, *Top++: A Program for the Calculation of the Top-Pair Cross-Section at Hadron Colliders*, *Comput. Phys. Commun.* **185** (2014) 2930 [arXiv:1112.5675] [INSPIRE].

[76] S. Alioli, P. Nason, C. Oleari and E. Re, *NLO single-top production matched with shower in POWHEG: s- and t-channel contributions*, *JHEP* **09** (2009) 111 [*Erratum ibid.* **02** (2010) 011] [arXiv:0907.4076] [INSPIRE].

[77] W. Beenakker, R. Hopker, M. Spira and P.M. Zerwas, *Squark and gluino production at hadron colliders*, *Nucl. Phys.* **B 492** (1997) 51 [hep-ph/9610490] [INSPIRE].

[78] A. Kulesza and L. Motyka, *Threshold resummation for squark-antisquark and gluino-pair production at the LHC*, *Phys. Rev. Lett.* **102** (2009) 111802 [arXiv:0807.2405] [INSPIRE].

[79] A. Kulesza and L. Motyka, *Soft gluon resummation for the production of gluino-gluino and squark-antisquark pairs at the LHC*, *Phys. Rev.* **D 80** (2009) 095004 [arXiv:0905.4749] [INSPIRE].

[80] W. Beenakker, S. Brensing, M. Krämer, A. Kulesza, E. Laenen and I. Niessen, *Soft-gluon resummation for squark and gluino hadroproduction*, *JHEP* **12** (2009) 041 [arXiv:0909.4418] [INSPIRE].

[81] W. Beenakker et al., *Squark and Gluino Hadroproduction*, *Int. J. Mod. Phys.* **A 26** (2011) 2637 [arXiv:1105.1110] [INSPIRE].

[82] C. Borschensky et al., *Squark and gluino production cross sections in pp collisions at $\sqrt{s} = 13, 14, 33$ and 100 TeV*, *Eur. Phys. J.* **C 74** (2014) 3174 [arXiv:1407.5066] [INSPIRE].

[83] P. Skands, S. Carrazza and J. Rojo, *Tuning PYTHIA 8.1: the Monash 2013 Tune*, *Eur. Phys. J.* **C 74** (2014) 3024 [arXiv:1404.5630] [INSPIRE].

[84] CMS collaboration, *Event generator tunes obtained from underlying event and multiparton scattering measurements*, *Eur. Phys. J.* **C 76** (2016) 155 [arXiv:1512.00815] [INSPIRE].

[85] A.C. Kraan, *Interactions of heavy stable hadronizing particles*, *Eur. Phys. J.* **C 37** (2004) 91 [hep-ex/0404001] [INSPIRE].

[86] R. Mackeprang and A. Rizzi, *Interactions of Coloured Heavy Stable Particles in Matter*, *Eur. Phys. J.* **C 50** (2007) 353 [hep-ph/0612161] [INSPIRE].

[87] O. Buchmueller et al., *Simplified Models for Displaced Dark Matter Signatures*, *JHEP* **09** (2017) 076 [arXiv:1704.06515] [INSPIRE].

[88] GEANT4 collaboration, S. Agostinelli et al., *GEANT4 — A Simulation toolkit*, *Nucl. Instrum. Meth.* **A 506** (2003) 250 [INSPIRE].

[89] CMS collaboration, *The fast simulation of the CMS detector at LHC*, *J. Phys. Conf. Ser.* **331** (2011) 032049 [INSPIRE].

[90] J. Butterworth et al., *PDF4LHC recommendations for LHC Run II*, *J. Phys.* **G 43** (2016) 023001 [arXiv:1510.03865] [INSPIRE].

[91] ATLAS collaboration, *Measurement of the Inelastic Proton-Proton Cross Section at $\sqrt{s} = 13$ TeV with the ATLAS Detector at the LHC*, *Phys. Rev. Lett.* **117** (2016) 182002 [arXiv:1606.02625] [INSPIRE].

[92] J.S. Conway, *Incorporating Nuisance Parameters in Likelihoods for Multisource Spectra*, in proceedings of *PHYSTAT 2011 Workshop on Statistical Issues Related to Discovery Claims in Search Experiments and Unfolding*, CERN,Geneva, Switzerland 17–20 January 2011, pp. 115–120 [DOI:10.5170/CERN-2011-006.115] [`arXiv:1103.0354`] [INSPIRE].

[93] ATLAS, CMS collaborations, LHC HIGGS COMBINATION GROUP, *Procedure for the LHC Higgs boson search combination in Summer 2011*, CMS-NOTE-2011-005; ATL-PHYS-PUB-2011-11 (2011).

[94] T. Junk, *Confidence level computation for combining searches with small statistics*, *Nucl. Instrum. Meth.* **A 434** (1999) 435 [`hep-ex/9902006`] [INSPIRE].

[95] A.L. Read, *Presentation of search results: The CL(s) technique*, *J. Phys.* **G 28** (2002) 2693 [INSPIRE].

[96] G. Cowan, K. Cranmer, E. Gross and O. Vitells, *Asymptotic formulae for likelihood-based tests of new physics*, *Eur. Phys. J.* **C 71** (2011) 1554 [*Erratum ibid.* **C 73** (2013) 2501] [`arXiv:1007.1727`] [INSPIRE].

The CMS collaboration

Yerevan Physics Institute, Yerevan, Armenia

A.M. Sirunyan, A. Tumasyan

Institut für Hochenergiephysik, Wien, Austria

W. Adam, F. Ambrogi, E. Asilar, T. Bergauer, J. Brandstetter, E. Brondolin, M. Dragicevic, J. Erö, A. Escalante Del Valle, M. Flechl, M. Friedl, R. Frühwirth[1], V.M. Ghete, J. Grossmann, J. Hrubec, M. Jeitler[1], A. König, N. Krammer, I. Krätschmer, D. Liko, T. Madlener, I. Mikulec, E. Pree, N. Rad, H. Rohringer, J. Schieck[1], R. Schöfbeck, M. Spanring, D. Spitzbart, A. Taurok, W. Waltenberger, J. Wittmann, C.-E. Wulz[1], M. Zarucki

Institute for Nuclear Problems, Minsk, Belarus

V. Chekhovsky, V. Mossolov, J. Suarez Gonzalez

Universiteit Antwerpen, Antwerpen, Belgium

E.A. De Wolf, D. Di Croce, X. Janssen, J. Lauwers, M. Pieters, M. Van De Klundert, H. Van Haevermaet, P. Van Mechelen, N. Van Remortel

Vrije Universiteit Brussel, Brussel, Belgium

S. Abu Zeid, F. Blekman, J. D'Hondt, I. De Bruyn, J. De Clercq, K. Deroover, G. Flouris, D. Lontkovskyi, S. Lowette, I. Marchesini, S. Moortgat, L. Moreels, Q. Python, K. Skovpen, S. Tavernier, W. Van Doninck, P. Van Mulders, I. Van Parijs

Université Libre de Bruxelles, Bruxelles, Belgium

D. Beghin, B. Bilin, H. Brun, B. Clerbaux, G. De Lentdecker, H. Delannoy, B. Dorney, G. Fasanella, L. Favart, R. Goldouzian, A. Grebenyuk, A.K. Kalsi, T. Lenzi, J. Luetic, T. Seva, E. Starling, C. Vander Velde, P. Vanlaer, D. Vannerom, R. Yonamine

Ghent University, Ghent, Belgium

T. Cornelis, D. Dobur, A. Fagot, M. Gul, I. Khvastunov[2], D. Poyraz, C. Roskas, D. Trocino, M. Tytgat, W. Verbeke, B. Vermassen, M. Vit, N. Zaganidis

Université Catholique de Louvain, Louvain-la-Neuve, Belgium

H. Bakhshiansohi, O. Bondu, S. Brochet, G. Bruno, C. Caputo, A. Caudron, P. David, S. De Visscher, C. Delaere, M. Delcourt, B. Francois, A. Giammanco, G. Krintiras, V. Lemaitre, A. Magitteri, A. Mertens, M. Musich, K. Piotrzkowski, L. Quertenmont, A. Saggio, M. Vidal Marono, S. Wertz, J. Zobec

Centro Brasileiro de Pesquisas Fisicas, Rio de Janeiro, Brazil

W.L. Aldá Júnior, F.L. Alves, G.A. Alves, L. Brito, G. Correia Silva, C. Hensel, A. Moraes, M.E. Pol, P. Rebello Teles

Universidade do Estado do Rio de Janeiro, Rio de Janeiro, Brazil

E. Belchior Batista Das Chagas, W. Carvalho, J. Chinellato[3], E. Coelho, E.M. Da Costa, G.G. Da Silveira[4], D. De Jesus Damiao, S. Fonseca De Souza, L.M. Huertas Guativa, H. Malbouisson, M. Medina Jaime[5], M. Melo De Almeida, C. Mora Herrera,

L. Mundim, H. Nogima, L.J. Sanchez Rosas, A. Santoro, A. Sznajder, M. Thiel, E.J. Tonelli Manganote[3], F. Torres Da Silva De Araujo, A. Vilela Pereira

Universidade Estadual Paulista [a]**, Universidade Federal do ABC** [b]**, São Paulo, Brazil**

S. Ahuja[a], C.A. Bernardes[a], L. Calligaris[a], T.R. Fernandez Perez Tomei[a], E.M. Gregores[b], P.G. Mercadante[b], S.F. Novaes[a], Sandra S. Padula[a], D. Romero Abad[b], J.C. Ruiz Vargas[a]

Institute for Nuclear Research and Nuclear Energy, Bulgarian Academy of Sciences, Sofia, Bulgaria

A. Aleksandrov, R. Hadjiiska, P. Iaydjiev, A. Marinov, M. Misheva, M. Rodozov, M. Shopova, G. Sultanov

University of Sofia, Sofia, Bulgaria

A. Dimitrov, L. Litov, B. Pavlov, P. Petkov

Beihang University, Beijing, China

W. Fang[6], X. Gao[6], L. Yuan

Institute of High Energy Physics, Beijing, China

M. Ahmad, J.G. Bian, G.M. Chen, H.S. Chen, M. Chen, Y. Chen, C.H. Jiang, D. Leggat, H. Liao, Z. Liu, F. Romeo, S.M. Shaheen, A. Spiezia, J. Tao, C. Wang, Z. Wang, E. Yazgan, H. Zhang, J. Zhao

State Key Laboratory of Nuclear Physics and Technology, Peking University, Beijing, China

Y. Ban, G. Chen, J. Li, Q. Li, S. Liu, Y. Mao, S.J. Qian, D. Wang, Z. Xu

Tsinghua University, Beijing, China

Y. Wang

Universidad de Los Andes, Bogota, Colombia

C. Avila, A. Cabrera, C.A. Carrillo Montoya, L.F. Chaparro Sierra, C. Florez, C.F. González Hernández, M.A. Segura Delgado

University of Split, Faculty of Electrical Engineering, Mechanical Engineering and Naval Architecture, Split, Croatia

B. Courbon, N. Godinovic, D. Lelas, I. Puljak, P.M. Ribeiro Cipriano, T. Sculac

University of Split, Faculty of Science, Split, Croatia

Z. Antunovic, M. Kovac

Institute Rudjer Boskovic, Zagreb, Croatia

V. Brigljevic, D. Ferencek, K. Kadija, B. Mesic, A. Starodumov[7], T. Susa

University of Cyprus, Nicosia, Cyprus

M.W. Ather, A. Attikis, G. Mavromanolakis, J. Mousa, C. Nicolaou, F. Ptochos, P.A. Razis, H. Rykaczewski

Charles University, Prague, Czech Republic

M. Finger[8], M. Finger Jr.[8]

Universidad San Francisco de Quito, Quito, Ecuador

E. Carrera Jarrin

Academy of Scientific Research and Technology of the Arab Republic of Egypt, Egyptian Network of High Energy Physics, Cairo, Egypt

A.A. Abdelalim[9,10], E. El-khateeb[11], S. Khalil[10]

National Institute of Chemical Physics and Biophysics, Tallinn, Estonia

S. Bhowmik, R.K. Dewanjee, M. Kadastik, L. Perrini, M. Raidal, C. Veelken

Department of Physics, University of Helsinki, Helsinki, Finland

P. Eerola, H. Kirschenmann, J. Pekkanen, M. Voutilainen

Helsinki Institute of Physics, Helsinki, Finland

J. Havukainen, J.K. Heikkilä, T. Järvinen, V. Karimäki, R. Kinnunen, T. Lampén, K. Lassila-Perini, S. Laurila, S. Lehti, T. Lindén, P. Luukka, T. Mäenpää, H. Siikonen, E. Tuominen, J. Tuominiemi

Lappeenranta University of Technology, Lappeenranta, Finland

T. Tuuva

IRFU, CEA, Université Paris-Saclay, Gif-sur-Yvette, France

M. Besancon, F. Couderc, M. Dejardin, D. Denegri, J.L. Faure, F. Ferri, S. Ganjour, S. Ghosh, A. Givernaud, P. Gras, G. Hamel de Monchenault, P. Jarry, C. Leloup, E. Locci, M. Machet, J. Malcles, G. Negro, J. Rander, A. Rosowsky, M.Ö. Sahin, M. Titov

Laboratoire Leprince-Ringuet, Ecole polytechnique, CNRS/IN2P3, Université Paris-Saclay, Palaiseau, France

A. Abdulsalam[12], C. Amendola, I. Antropov, S. Baffioni, F. Beaudette, P. Busson, L. Cadamuro, C. Charlot, R. Granier de Cassagnac, M. Jo, I. Kucher, S. Lisniak, A. Lobanov, J. Martin Blanco, M. Nguyen, C. Ochando, G. Ortona, P. Paganini, P. Pigard, R. Salerno, J.B. Sauvan, Y. Sirois, A.G. Stahl Leiton, Y. Yilmaz, A. Zabi, A. Zghiche

Université de Strasbourg, CNRS, IPHC UMR 7178, F-67000 Strasbourg, France

J.-L. Agram[13], J. Andrea, D. Bloch, J.-M. Brom, M. Buttignol, E.C. Chabert, C. Collard, E. Conte[13], X. Coubez, F. Drouhin[13], J.-C. Fontaine[13], D. Gelé, U. Goerlach, M. Jansová, P. Juillot, A.-C. Le Bihan, N. Tonon, P. Van Hove

Centre de Calcul de l'Institut National de Physique Nucleaire et de Physique des Particules, CNRS/IN2P3, Villeurbanne, France

S. Gadrat

Université de Lyon, Université Claude Bernard Lyon 1, CNRS-IN2P3, Institut de Physique Nucléaire de Lyon, Villeurbanne, France

S. Beauceron, C. Bernet, G. Boudoul, N. Chanon, R. Chierici, D. Contardo, P. Depasse, H. El Mamouni, J. Fay, L. Finco, S. Gascon, M. Gouzevitch, G. Grenier, B. Ille, F. Lagarde, I.B. Laktineh, H. Lattaud, M. Lethuillier, L. Mirabito, A.L. Pequegnot, S. Perries, A. Popov[14], V. Sordini, M. Vander Donckt, S. Viret, S. Zhang

Georgian Technical University, Tbilisi, Georgia

T. Toriashvili[15]

Tbilisi State University, Tbilisi, Georgia

Z. Tsamalaidze[8]

RWTH Aachen University, I. Physikalisches Institut, Aachen, Germany

C. Autermann, L. Feld, M.K. Kiesel, K. Klein, M. Lipinski, M. Preuten, C. Schomakers, J. Schulz, M. Teroerde, B. Wittmer, V. Zhukov[14]

RWTH Aachen University, III. Physikalisches Institut A, Aachen, Germany

A. Albert, D. Duchardt, M. Endres, M. Erdmann, S. Erdweg, T. Esch, R. Fischer, A. Güth, T. Hebbeker, C. Heidemann, K. Hoepfner, S. Knutzen, M. Merschmeyer, A. Meyer, P. Millet, S. Mukherjee, T. Pook, M. Radziej, H. Reithler, M. Rieger, F. Scheuch, D. Teyssier, S. Thüer

RWTH Aachen University, III. Physikalisches Institut B, Aachen, Germany

G. Flügge, B. Kargoll, T. Kress, A. Künsken, T. Müller, A. Nehrkorn, A. Nowack, C. Pistone, O. Pooth, A. Stahl[16]

Deutsches Elektronen-Synchrotron, Hamburg, Germany

M. Aldaya Martin, T. Arndt, C. Asawatangtrakuldee, K. Beernaert, O. Behnke, U. Behrens, A. Bermúdez Martínez, A.A. Bin Anuar, K. Borras[17], V. Botta, A. Campbell, P. Connor, C. Contreras-Campana, F. Costanza, V. Danilov, A. De Wit, C. Diez Pardos, D. Domínguez Damiani, G. Eckerlin, D. Eckstein, T. Eichhorn, E. Eren, E. Gallo[18], J. Garay Garcia, A. Geiser, J.M. Grados Luyando, A. Grohsjean, P. Gunnellini, M. Guthoff, A. Harb, J. Hauk, M. Hempel[19], H. Jung, M. Kasemann, J. Keaveney, C. Kleinwort, J. Knolle, I. Korol, D. Krücker, W. Lange, A. Lelek, T. Lenz, K. Lipka, W. Lohmann[19], R. Mankel, I.-A. Melzer-Pellmann, A.B. Meyer, M. Meyer, M. Missiroli, G. Mittag, J. Mnich, A. Mussgiller, D. Pitzl, A. Raspereza, M. Savitskyi, P. Saxena, R. Shevchenko, N. Stefaniuk, H. Tholen, G.P. Van Onsem, R. Walsh, Y. Wen, K. Wichmann, C. Wissing, O. Zenaiev

University of Hamburg, Hamburg, Germany

R. Aggleton, S. Bein, V. Blobel, M. Centis Vignali, T. Dreyer, E. Garutti, D. Gonzalez, J. Haller, A. Hinzmann, M. Hoffmann, A. Karavdina, G. Kasieczka, R. Klanner, R. Kogler, N. Kovalchuk, S. Kurz, D. Marconi, J. Multhaup, M. Niedziela, D. Nowatschin, T. Peiffer, A. Perieanu, A. Reimers, C. Scharf, P. Schleper, A. Schmidt, S. Schumann, J. Schwandt, J. Sonneveld, H. Stadie, G. Steinbrück, F.M. Stober, M. Stöver, D. Troendle, E. Usai, A. Vanhoefer, B. Vormwald

Institut für Experimentelle Teilchenphysik, Karlsruhe, Germany

M. Akbiyik, C. Barth, M. Baselga, S. Baur, E. Butz, R. Caspart, T. Chwalek, F. Colombo, W. De Boer, A. Dierlamm, N. Faltermann, B. Freund, R. Friese, M. Giffels, M.A. Harrendorf, F. Hartmann[16], S.M. Heindl, U. Husemann, F. Kassel[16], S. Kudella, H. Mildner, M.U. Mozer, Th. Müller, M. Plagge, G. Quast, K. Rabbertz, M. Schröder, I. Shvetsov,

G. Sieber, H.J. Simonis, R. Ulrich, S. Wayand, M. Weber, T. Weiler, S. Williamson, C. Wöhrmann, R. Wolf

Institute of Nuclear and Particle Physics (INPP), NCSR Demokritos, Aghia Paraskevi, Greece

G. Anagnostou, G. Daskalakis, T. Geralis, A. Kyriakis, D. Loukas, I. Topsis-Giotis

National and Kapodistrian University of Athens, Athens, Greece

G. Karathanasis, S. Kesisoglou, A. Panagiotou, N. Saoulidou, E. Tziaferi

National Technical University of Athens, Athens, Greece

K. Kousouris, I. Papakrivopoulos

University of Ioánnina, Ioánnina, Greece

I. Evangelou, C. Foudas, P. Gianneios, P. Katsoulis, P. Kokkas, S. Mallios, N. Manthos, I. Papadopoulos, E. Paradas, J. Strologas, F.A. Triantis, D. Tsitsonis

MTA-ELTE Lendület CMS Particle and Nuclear Physics Group, Eötvös Loránd University, Budapest, Hungary

M. Csanad, N. Filipovic, G. Pasztor, O. Surányi, G.I. Veres[20]

Wigner Research Centre for Physics, Budapest, Hungary

G. Bencze, C. Hajdu, D. Horvath[21], Á. Hunyadi, F. Sikler, V. Veszpremi, G. Vesztergombi[20], T.Á. Vámi

Institute of Nuclear Research ATOMKI, Debrecen, Hungary

N. Beni, S. Czellar, J. Karancsi[22], A. Makovec, J. Molnar, Z. Szillasi

Institute of Physics, University of Debrecen, Debrecen, Hungary

M. Bartók[20], P. Raics, Z.L. Trocsanyi, B. Ujvari

Indian Institute of Science (IISc), Bangalore, India

S. Choudhury, J.R. Komaragiri

National Institute of Science Education and Research, Bhubaneswar, India

S. Bahinipati[23], P. Mal, K. Mandal, A. Nayak[24], D.K. Sahoo[23], N. Sahoo, S.K. Swain

Panjab University, Chandigarh, India

S. Bansal, S.B. Beri, V. Bhatnagar, S. Chauhan, R. Chawla, N. Dhingra, R. Gupta, A. Kaur, M. Kaur, S. Kaur, R. Kumar, P. Kumari, M. Lohan, A. Mehta, S. Sharma, J.B. Singh, G. Walia

University of Delhi, Delhi, India

Ashok Kumar, Aashaq Shah, A. Bhardwaj, B.C. Choudhary, R.B. Garg, S. Keshri, A. Kumar, S. Malhotra, M. Naimuddin, K. Ranjan, R. Sharma

Saha Institute of Nuclear Physics, HBNI, Kolkata, India

R. Bhardwaj[25], R. Bhattacharya, S. Bhattacharya, U. Bhawandeep[25], D. Bhowmik, S. Dey, S. Dutt[25], S. Dutta, S. Ghosh, N. Majumdar, K. Mondal, S. Mukhopadhyay, S. Nandan, A. Purohit, P.K. Rout, A. Roy, S. Roy Chowdhury, S. Sarkar, M. Sharan, B. Singh, S. Thakur[25]

Indian Institute of Technology Madras, Madras, India

P.K. Behera

Bhabha Atomic Research Centre, Mumbai, India

R. Chudasama, D. Dutta, V. Jha, V. Kumar, A.K. Mohanty[16], P.K. Netrakanti, L.M. Pant, P. Shukla, A. Topkar

Tata Institute of Fundamental Research-A, Mumbai, India

T. Aziz, S. Dugad, B. Mahakud, S. Mitra, G.B. Mohanty, N. Sur, B. Sutar

Tata Institute of Fundamental Research-B, Mumbai, India

S. Banerjee, S. Bhattacharya, S. Chatterjee, P. Das, M. Guchait, Sa. Jain, S. Kumar, M. Maity[26], G. Majumder, K. Mazumdar, T. Sarkar[26], N. Wickramage[27]

Indian Institute of Science Education and Research (IISER), Pune, India

S. Chauhan, S. Dube, V. Hegde, A. Kapoor, K. Kothekar, S. Pandey, A. Rane, S. Sharma

Institute for Research in Fundamental Sciences (IPM), Tehran, Iran

S. Chenarani[28], E. Eskandari Tadavani, S.M. Etesami[28], M. Khakzad, M. Mohammadi Najafabadi, M. Naseri, S. Paktinat Mehdiabadi[29], F. Rezaei Hosseinabadi, B. Safarzadeh[30], M. Zeinali

University College Dublin, Dublin, Ireland

M. Felcini, M. Grunewald

INFN Sezione di Bari [a], Università di Bari [b], Politecnico di Bari [c], Bari, Italy

M. Abbrescia[a,b], C. Calabria[a,b], A. Colaleo[a], D. Creanza[a,c], L. Cristella[a,b], N. De Filippis[a,c], M. De Palma[a,b], A. Di Florio[a,b], F. Errico[a,b], L. Fiore[a], A. Gelmi[a,b], G. Iaselli[a,c], S. Lezki[a,b], G. Maggi[a,c], M. Maggi[a], B. Marangelli[a,b], G. Miniello[a,b], S. My[a,b], S. Nuzzo[a,b], A. Pompili[a,b], G. Pugliese[a,c], R. Radogna[a], A. Ranieri[a], G. Selvaggi[a,b], A. Sharma[a], L. Silvestris[a,16], R. Venditti[a], P. Verwilligen[a], G. Zito[a]

INFN Sezione di Bologna [a], Università di Bologna [b], Bologna, Italy

G. Abbiendi[a], C. Battilana[a,b], D. Bonacorsi[a,b], L. Borgonovi[a,b], S. Braibant-Giacomelli[a,b], L. Brigliadori[a,b], R. Campanini[a,b], P. Capiluppi[a,b], A. Castro[a,b], F.R. Cavallo[a], S.S. Chhibra[a,b], G. Codispoti[a,b], M. Cuffiani[a,b], G.M. Dallavalle[a], F. Fabbri[a], A. Fanfani[a,b], D. Fasanella[a,b], P. Giacomelli[a], C. Grandi[a], L. Guiducci[a,b], F. Iemmi, S. Marcellini[a], G. Masetti[a], A. Montanari[a], F.L. Navarria[a,b], A. Perrotta[a], T. Rovelli[a,b], G.P. Siroli[a,b], N. Tosi[a]

INFN Sezione di Catania [a], Università di Catania [b], Catania, Italy

S. Albergo[a,b], S. Costa[a,b], A. Di Mattia[a], F. Giordano[a,b], R. Potenza[a,b], A. Tricomi[a,b], C. Tuve[a,b]

INFN Sezione di Firenze [a], Università di Firenze [b], Firenze, Italy

G. Barbagli[a], K. Chatterjee[a,b], V. Ciulli[a,b], C. Civinini[a], R. D'Alessandro[a,b], E. Focardi[a,b], G. Latino, P. Lenzi[a,b], M. Meschini[a], S. Paoletti[a], L. Russo[a,31], G. Sguazzoni[a], D. Strom[a], L. Viliani[a]

INFN Laboratori Nazionali di Frascati, Frascati, Italy

L. Benussi, S. Bianco, F. Fabbri, D. Piccolo, F. Primavera[16]

INFN Sezione di Genova [a]**, Università di Genova** [b]**, Genova, Italy**

V. Calvelli[a,b], F. Ferro[a], F. Ravera[a,b], E. Robutti[a], S. Tosi[a,b]

INFN Sezione di Milano-Bicocca [a]**, Università di Milano-Bicocca** [b]**, Milano, Italy**

A. Benaglia[a], A. Beschi[b], L. Brianza[a,b], F. Brivio[a,b], V. Ciriolo[a,b,16], M.E. Dinardo[a,b], S. Fiorendi[a,b], S. Gennai[a], A. Ghezzi[a,b], P. Govoni[a,b], M. Malberti[a,b], S. Malvezzi[a], R.A. Manzoni[a,b], D. Menasce[a], L. Moroni[a], M. Paganoni[a,b], K. Pauwels[a,b], D. Pedrini[a], S. Pigazzini[a,b,32], S. Ragazzi[a,b], T. Tabarelli de Fatis[a,b]

INFN Sezione di Napoli [a]**, Università di Napoli 'Federico II'** [b]**, Napoli, Italy, Università della Basilicata** [c]**, Potenza, Italy, Università G. Marconi** [d]**, Roma, Italy**

S. Buontempo[a], N. Cavallo[a,c], S. Di Guida[a,d,16], F. Fabozzi[a,c], F. Fienga[a,b], G. Galati[a,b], A.O.M. Iorio[a,b], W.A. Khan[a], L. Lista[a], S. Meola[a,d,16], P. Paolucci[a,16], C. Sciacca[a,b], F. Thyssen[a], E. Voevodina[a,b]

INFN Sezione di Padova [a]**, Università di Padova** [b]**, Padova, Italy, Università di Trento** [c]**, Trento, Italy**

P. Azzi[a], N. Bacchetta[a], L. Benato[a,b], D. Bisello[a,b], A. Boletti[a,b], R. Carlin[a,b], A. Carvalho Antunes De Oliveira[a,b], P. Checchia[a], P. De Castro Manzano[a], T. Dorigo[a], U. Dosselli[a], F. Gasparini[a,b], U. Gasparini[a,b], A. Gozzelino[a], S. Lacaprara[a], M. Margoni[a,b], A.T. Meneguzzo[a,b], N. Pozzobon[a,b], P. Ronchese[a,b], R. Rossin[a,b], F. Simonetto[a,b], A. Tiko, E. Torassa[a], M. Zanetti[a,b], P. Zotto[a,b], G. Zumerle[a,b]

INFN Sezione di Pavia [a]**, Università di Pavia** [b]**, Pavia, Italy**

A. Braghieri[a], A. Magnani[a], P. Montagna[a,b], S.P. Ratti[a,b], V. Re[a], M. Ressegotti[a,b], C. Riccardi[a,b], P. Salvini[a], I. Vai[a,b], P. Vitulo[a,b]

INFN Sezione di Perugia [a]**, Università di Perugia** [b]**, Perugia, Italy**

L. Alunni Solestizi[a,b], M. Biasini[a,b], G.M. Bilei[a], C. Cecchi[a,b], D. Ciangottini[a,b], L. Fanò[a,b], P. Lariccia[a,b], R. Leonardi[a,b], E. Manoni[a], G. Mantovani[a,b], V. Mariani[a,b], M. Menichelli[a], A. Rossi[a,b], A. Santocchia[a,b], D. Spiga[a]

INFN Sezione di Pisa [a]**, Università di Pisa** [b]**, Scuola Normale Superiore di Pisa** [c]**, Pisa, Italy**

K. Androsov[a], P. Azzurri[a,16], G. Bagliesi[a], L. Bianchini[a], T. Boccali[a], L. Borrello, R. Castaldi[a], M.A. Ciocci[a,b], R. Dell'Orso[a], G. Fedi[a], L. Giannini[a,c], A. Giassi[a], M.T. Grippo[a,31], F. Ligabue[a,c], T. Lomtadze[a], E. Manca[a,c], G. Mandorli[a,c], A. Messineo[a,b], F. Palla[a], A. Rizzi[a,b], P. Spagnolo[a], R. Tenchini[a], G. Tonelli[a,b], A. Venturi[a], P.G. Verdini[a]

INFN Sezione di Roma [a]**, Sapienza Università di Roma** [b]**, Rome, Italy**

L. Barone[a,b], F. Cavallari[a], M. Cipriani[a,b], N. Daci[a], D. Del Re[a,b], E. Di Marco[a,b], M. Diemoz[a], S. Gelli[a,b], E. Longo[a,b], F. Margaroli[a,b], B. Marzocchi[a,b], P. Meridiani[a],

G. Organtini^{a,b}, F. Pandolfi^a, R. Paramatti^{a,b}, F. Preiato^{a,b}, S. Rahatlou^{a,b}, C. Rovelli^a, F. Santanastasio^{a,b}

INFN Sezione di Torino ^{a}, Università di Torino ^{b}, Torino, Italy, Università del Piemonte Orientale ^{c}, Novara, Italy

N. Amapane^{a,b}, R. Arcidiacono^{a,c}, S. Argiro^{a,b}, M. Arneodo^{a,c}, N. Bartosik^a, R. Bellan^{a,b}, C. Biino^a, N. Cartiglia^a, R. Castello^{a,b}, F. Cenna^{a,b}, M. Costa^{a,b}, R. Covarelli^{a,b}, A. Degano^{a,b}, N. Demaria^a, B. Kiani^{a,b}, C. Mariotti^a, S. Maselli^a, E. Migliore^{a,b}, V. Monaco^{a,b}, E. Monteil^{a,b}, M. Monteno^a, M.M. Obertino^{a,b}, L. Pacher^{a,b}, N. Pastrone^a, M. Pelliccioni^a, G.L. Pinna Angioni^{a,b}, A. Romero^{a,b}, M. Ruspa^{a,c}, R. Sacchi^{a,b}, K. Shchelina^{a,b}, V. Sola^a, A. Solano^{a,b}, A. Staiano^a

INFN Sezione di Trieste ^{a}, Università di Trieste ^{b}, Trieste, Italy

S. Belforte^a, M. Casarsa^a, F. Cossutti^a, G. Della Ricca^{a,b}, A. Zanetti^a

Kyungpook National University

D.H. Kim, G.N. Kim, M.S. Kim, J. Lee, S. Lee, S.W. Lee, C.S. Moon, Y.D. Oh, S. Sekmen, D.C. Son, Y.C. Yang

Chonnam National University, Institute for Universe and Elementary Particles, Kwangju, Korea

H. Kim, D.H. Moon, G. Oh

Hanyang University, Seoul, Korea

J.A. Brochero Cifuentes, J. Goh, T.J. Kim

Korea University, Seoul, Korea

S. Cho, S. Choi, Y. Go, D. Gyun, S. Ha, B. Hong, Y. Jo, Y. Kim, K. Lee, K.S. Lee, S. Lee, J. Lim, S.K. Park, Y. Roh

Seoul National University, Seoul, Korea

J. Almond, J. Kim, J.S. Kim, H. Lee, K. Lee, K. Nam, S.B. Oh, B.C. Radburn-Smith, S.h. Seo, U.K. Yang, H.D. Yoo, G.B. Yu

University of Seoul, Seoul, Korea

H. Kim, J.H. Kim, J.S.H. Lee, I.C. Park

Sungkyunkwan University, Suwon, Korea

Y. Choi, C. Hwang, J. Lee, I. Yu

Vilnius University, Vilnius, Lithuania

V. Dudenas, A. Juodagalvis, J. Vaitkus

National Centre for Particle Physics, Universiti Malaya, Kuala Lumpur, Malaysia

I. Ahmed, Z.A. Ibrahim, M.A.B. Md Ali[33], F. Mohamad Idris[34], W.A.T. Wan Abdullah, M.N. Yusli, Z. Zolkapli

Centro de Investigacion y de Estudios Avanzados del IPN, Mexico City, Mexico

Reyes-Almanza, R, Ramirez-Sanchez, G., Duran-Osuna, M. C., H. Castilla-Valdez, E. De La Cruz-Burelo, I. Heredia-De La Cruz[35], Rabadan-Trejo, R. I., R. Lopez-Fernandez, J. Mejia Guisao, A. Sanchez-Hernandez

Universidad Iberoamericana, Mexico City, Mexico

S. Carrillo Moreno, C. Oropeza Barrera, F. Vazquez Valencia

Benemerita Universidad Autonoma de Puebla, Puebla, Mexico

J. Eysermans, I. Pedraza, H.A. Salazar Ibarguen, C. Uribe Estrada

Universidad Autónoma de San Luis Potosí, San Luis Potosí, Mexico

A. Morelos Pineda

University of Auckland, Auckland, New Zealand

D. Krofcheck

University of Canterbury, Christchurch, New Zealand

P.H. Butler

National Centre for Physics, Quaid-I-Azam University, Islamabad, Pakistan

A. Ahmad, M. Ahmad, Q. Hassan, H.R. Hoorani, A. Saddique, M.A. Shah, M. Shoaib, M. Waqas

National Centre for Nuclear Research, Swierk, Poland

H. Bialkowska, M. Bluj, B. Boimska, T. Frueboes, M. Górski, M. Kazana, K. Nawrocki, M. Szleper, P. Traczyk, P. Zalewski

Institute of Experimental Physics, Faculty of Physics, University of Warsaw, Warsaw, Poland

K. Bunkowski, A. Byszuk[36], K. Doroba, A. Kalinowski, M. Konecki, J. Krolikowski, M. Misiura, M. Olszewski, A. Pyskir, M. Walczak

Laboratório de Instrumentação e Física Experimental de Partículas, Lisboa, Portugal

P. Bargassa, C. Beirão Da Cruz E Silva, A. Di Francesco, P. Faccioli, B. Galinhas, M. Gallinaro, J. Hollar, N. Leonardo, L. Lloret Iglesias, M.V. Nemallapudi, J. Seixas, G. Strong, O. Toldaiev, D. Vadruccio, J. Varela

Joint Institute for Nuclear Research, Dubna, Russia

S. Afanasiev, P. Bunin, M. Gavrilenko, I. Golutvin, I. Gorbunov, A. Kamenev, V. Karjavin, A. Lanev, A. Malakhov, V. Matveev[37,38], P. Moisenz, V. Palichik, V. Perelygin, S. Shmatov, S. Shulha, N. Skatchkov, V. Smirnov, N. Voytishin, A. Zarubin

Petersburg Nuclear Physics Institute, Gatchina (St. Petersburg), Russia

Y. Ivanov, V. Kim[39], E. Kuznetsova[40], P. Levchenko, V. Murzin, V. Oreshkin, I. Smirnov, D. Sosnov, V. Sulimov, L. Uvarov, S. Vavilov, A. Vorobyev

Institute for Nuclear Research, Moscow, Russia

Yu. Andreev, A. Dermenev, S. Gninenko, N. Golubev, A. Karneyeu, M. Kirsanov, N. Krasnikov, A. Pashenkov, D. Tlisov, A. Toropin

Institute for Theoretical and Experimental Physics, Moscow, Russia

V. Epshteyn, V. Gavrilov, N. Lychkovskaya, V. Popov, I. Pozdnyakov, G. Safronov, A. Spiridonov, A. Stepennov, V. Stolin, M. Toms, E. Vlasov, A. Zhokin

Moscow Institute of Physics and Technology, Moscow, Russia

T. Aushev, A. Bylinkin[38]

National Research Nuclear University 'Moscow Engineering Physics Institute' (MEPhI), Moscow, Russia

M. Chadeeva[41], P. Parygin, D. Philippov, S. Polikarpov, E. Popova, V. Rusinov

P.N. Lebedev Physical Institute, Moscow, Russia

V. Andreev, M. Azarkin[38], I. Dremin[38], M. Kirakosyan[38], S.V. Rusakov, A. Terkulov

Skobeltsyn Institute of Nuclear Physics, Lomonosov Moscow State University, Moscow, Russia

A. Baskakov, A. Belyaev, E. Boos, M. Dubinin[42], L. Dudko, A. Ershov, A. Gribushin, V. Klyukhin, O. Kodolova, I. Lokhtin, I. Miagkov, S. Obraztsov, S. Petrushanko, V. Savrin, A. Snigirev

Novosibirsk State University (NSU), Novosibirsk, Russia

V. Blinov[43], D. Shtol[43], Y. Skovpen[43]

State Research Center of Russian Federation, Institute for High Energy Physics of NRC "Kurchatov Institute", Protvino, Russia

I. Azhgirey, I. Bayshev, S. Bitioukov, D. Elumakhov, A. Godizov, V. Kachanov, A. Kalinin, D. Konstantinov, P. Mandrik, V. Petrov, R. Ryutin, A. Sobol, S. Troshin, N. Tyurin, A. Uzunian, A. Volkov

National Research Tomsk Polytechnic University, Tomsk, Russia

A. Babaev

University of Belgrade, Faculty of Physics and Vinca Institute of Nuclear Sciences, Belgrade, Serbia

P. Adzic[44], P. Cirkovic, D. Devetak, M. Dordevic, J. Milosevic

Centro de Investigaciones Energéticas Medioambientales y Tecnológicas (CIEMAT), Madrid, Spain

J. Alcaraz Maestre, I. Bachiller, M. Barrio Luna, M. Cerrada, N. Colino, B. De La Cruz, A. Delgado Peris, C. Fernandez Bedoya, J.P. Fernández Ramos, J. Flix, M.C. Fouz, O. Gonzalez Lopez, S. Goy Lopez, J.M. Hernandez, M.I. Josa, D. Moran, A. Pérez-Calero Yzquierdo, J. Puerta Pelayo, I. Redondo, L. Romero, M.S. Soares, A. Triossi, A. Álvarez Fernández

Universidad Autónoma de Madrid, Madrid, Spain

C. Albajar, J.F. de Trocóniz

Universidad de Oviedo, Oviedo, Spain

J. Cuevas, C. Erice, J. Fernandez Menendez, S. Folgueras, I. Gonzalez Caballero, J.R. González Fernández, E. Palencia Cortezon, S. Sanchez Cruz, P. Vischia, J.M. Vizan Garcia

Instituto de Física de Cantabria (IFCA), CSIC-Universidad de Cantabria, Santander, Spain

I.J. Cabrillo, A. Calderon, B. Chazin Quero, J. Duarte Campderros, M. Fernandez, P.J. Fernández Manteca, J. Garcia-Ferrero, A. García Alonso, G. Gomez, A. Lopez Virto, J. Marco, C. Martinez Rivero, P. Martinez Ruiz del Arbol, F. Matorras, J. Piedra Gomez, C. Prieels, T. Rodrigo, A. Ruiz-Jimeno, L. Scodellaro, N. Trevisani, I. Vila, R. Vilar Cortabitarte

CERN, European Organization for Nuclear Research, Geneva, Switzerland

D. Abbaneo, B. Akgun, E. Auffray, P. Baillon, A.H. Ball, D. Barney, J. Bendavid, M. Bianco, A. Bocci, C. Botta, T. Camporesi, M. Cepeda, G. Cerminara, E. Chapon, Y. Chen, D. d'Enterria, A. Dabrowski, V. Daponte, A. David, M. De Gruttola, A. De Roeck, N. Deelen, M. Dobson, T. du Pree, M. Dünser, N. Dupont, A. Elliott-Peisert, P. Everaerts, F. Fallavollita[45], G. Franzoni, J. Fulcher, W. Funk, D. Gigi, A. Gilbert, K. Gill, F. Glege, D. Gulhan, J. Hegeman, V. Innocente, A. Jafari, P. Janot, O. Karacheban[19], J. Kieseler, V. Knünz, A. Kornmayer, M. Krammer[1], C. Lange, P. Lecoq, C. Lourenço, M.T. Lucchini, L. Malgeri, M. Mannelli, A. Martelli, F. Meijers, J.A. Merlin, S. Mersi, E. Meschi, P. Milenovic[46], F. Moortgat, M. Mulders, H. Neugebauer, J. Ngadiuba, S. Orfanelli, L. Orsini, F. Pantaleo[16], L. Pape, E. Perez, M. Peruzzi, A. Petrilli, G. Petrucciani, A. Pfeiffer, M. Pierini, F.M. Pitters, D. Rabady, A. Racz, T. Reis, G. Rolandi[47], M. Rovere, H. Sakulin, C. Schäfer, C. Schwick, M. Seidel, M. Selvaggi, A. Sharma, P. Silva, P. Sphicas[48], A. Stakia, J. Steggemann, M. Stoye, M. Tosi, D. Treille, A. Tsirou, V. Veckalns[49], M. Verweij, W.D. Zeuner

Paul Scherrer Institut, Villigen, Switzerland

W. Bertl[†], L. Caminada[50], K. Deiters, W. Erdmann, R. Horisberger, Q. Ingram, H.C. Kaestli, D. Kotlinski, U. Langenegger, T. Rohe, S.A. Wiederkehr

ETH Zurich - Institute for Particle Physics and Astrophysics (IPA), Zurich, Switzerland

M. Backhaus, L. Bäni, P. Berger, B. Casal, N. Chernyavskaya, G. Dissertori, M. Dittmar, M. Donegà, C. Dorfer, C. Grab, C. Heidegger, D. Hits, J. Hoss, T. Klijnsma, W. Lustermann, M. Marionneau, M.T. Meinhard, D. Meister, F. Micheli, P. Musella, F. Nessi-Tedaldi, J. Pata, F. Pauss, G. Perrin, L. Perrozzi, M. Quittnat, M. Reichmann, D. Ruini, D.A. Sanz Becerra, M. Schönenberger, L. Shchutska, V.R. Tavolaro, K. Theofilatos, M.L. Vesterbacka Olsson, R. Wallny, D.H. Zhu

Universität Zürich, Zurich, Switzerland

T.K. Aarrestad, C. Amsler[51], D. Brzhechko, M.F. Canelli, A. De Cosa, R. Del Burgo, S. Donato, C. Galloni, T. Hreus, B. Kilminster, I. Neutelings, D. Pinna, G. Rauco, P. Robmann, D. Salerno, K. Schweiger, C. Seitz, Y. Takahashi, A. Zucchetta

National Central University, Chung-Li, Taiwan

V. Candelise, Y.H. Chang, K.y. Cheng, T.H. Doan, Sh. Jain, R. Khurana, C.M. Kuo, W. Lin, A. Pozdnyakov, S.S. Yu

National Taiwan University (NTU), Taipei, Taiwan

Arun Kumar, P. Chang, Y. Chao, K.F. Chen, P.H. Chen, F. Fiori, W.-S. Hou, Y. Hsiung, Y.F. Liu, R.-S. Lu, E. Paganis, A. Psallidas, A. Steen, J.f. Tsai

Chulalongkorn University, Faculty of Science, Department of Physics, Bangkok, Thailand

B. Asavapibhop, K. Kovitanggoon, G. Singh, N. Srimanobhas

Çukurova University, Physics Department, Science and Art Faculty, Adana, Turkey

A. Bat, F. Boran, S. Cerci[52], S. Damarseckin, Z.S. Demiroglu, C. Dozen, I. Dumanoglu, S. Girgis, G. Gokbulut, Y. Guler, I. Hos[53], E.E. Kangal[54], O. Kara, U. Kiminsu, M. Oglakci, G. Onengut, K. Ozdemir[55], D. Sunar Cerci[52], B. Tali[52], U.G. Tok, H. Topakli[56], S. Turkcapar, I.S. Zorbakir, C. Zorbilmez

Middle East Technical University, Physics Department, Ankara, Turkey

G. Karapinar[57], K. Ocalan[58], M. Yalvac, M. Zeyrek

Bogazici University, Istanbul, Turkey

E. Gülmez, M. Kaya[59], O. Kaya[60], S. Tekten, E.A. Yetkin[61]

Istanbul Technical University, Istanbul, Turkey

M.N. Agaras, S. Atay, A. Cakir, K. Cankocak, Y. Komurcu

Institute for Scintillation Materials of National Academy of Science of Ukraine, Kharkov, Ukraine

B. Grynyov

National Scientific Center, Kharkov Institute of Physics and Technology, Kharkov, Ukraine

L. Levchuk

University of Bristol, Bristol, United Kingdom

F. Ball, L. Beck, E. Bhal, J.J. Brooke, D. Burns, E. Clement, D. Cussans, O. Davignon, H. Flacher, J. Goldstein, G.P. Heath, H.F. Heath, L. Kreczko, B. Krikler, D.M. Newbold[62], S. Paramesvaran, T. Sakuma, S. Seif El Nasr-storey, D. Smith, V.J. Smith

Rutherford Appleton Laboratory, Didcot, United Kingdom

K.W. Bell, A. Belyaev[63], C. Brew, R.M. Brown, D. Cieri, D.J.A. Cockerill, J.A. Coughlan, K. Harder, S. Harper, J. Linacre, E. Olaiya, D. Petyt, C.H. Shepherd-Themistocleous, A. Thea, I.R. Tomalin, T. Williams, W.J. Womersley

Imperial College, London, United Kingdom

G. Auzinger, R. Bainbridge, P. Bloch, J. Borg, S. Breeze, O. Buchmuller, A. Bundock, S. Casasso, D. Colling, L. Corpe, P. Dauncey, G. Davies, M. Della Negra, R. Di Maria, A. Elwood, Y. Haddad, G. Hall, G. Iles, T. James, M. Komm, R. Lane, C. Laner, L. Lyons, A.-M. Magnan, S. Malik, L. Mastrolorenzo, T. Matsushita, J. Nash[64], A. Nikitenko[7], V. Palladino, M. Pesaresi, A. Richards, A. Rose, E. Scott, C. Seez, A. Shtipliyski, T. Strebler, S. Summers, A. Tapper, K. Uchida, M. Vazquez Acosta[65], T. Virdee[16], N. Wardle, D. Winterbottom, J. Wright, S.C. Zenz

Brunel University, Uxbridge, United Kingdom

J.E. Cole, P.R. Hobson, A. Khan, P. Kyberd, A. Morton, I.D. Reid, L. Teodorescu, S. Zahid

Baylor University, Waco, U.S.A.

A. Borzou, K. Call, J. Dittmann, K. Hatakeyama, H. Liu, N. Pastika, C. Smith

Catholic University of America, Washington DC, U.S.A.

R. Bartek, A. Dominguez

The University of Alabama, Tuscaloosa, U.S.A.

A. Buccilli, S.I. Cooper, C. Henderson, P. Rumerio, C. West

Boston University, Boston, U.S.A.

D. Arcaro, A. Avetisyan, T. Bose, D. Gastler, D. Rankin, C. Richardson, J. Rohlf, L. Sulak, D. Zou

Brown University, Providence, U.S.A.

G. Benelli, D. Cutts, M. Hadley, J. Hakala, U. Heintz, J.M. Hogan[66], K.H.M. Kwok, E. Laird, G. Landsberg, J. Lee, Z. Mao, M. Narain, J. Pazzini, S. Piperov, S. Sagir, R. Syarif, D. Yu

University of California, Davis, Davis, U.S.A.

R. Band, C. Brainerd, R. Breedon, D. Burns, M. Calderon De La Barca Sanchez, M. Chertok, J. Conway, R. Conway, P.T. Cox, R. Erbacher, C. Flores, G. Funk, W. Ko, R. Lander, C. Mclean, M. Mulhearn, D. Pellett, J. Pilot, S. Shalhout, M. Shi, J. Smith, D. Stolp, D. Taylor, K. Tos, M. Tripathi, Z. Wang, F. Zhang

University of California, Los Angeles, U.S.A.

M. Bachtis, C. Bravo, R. Cousins, A. Dasgupta, A. Florent, J. Hauser, M. Ignatenko, N. Mccoll, S. Regnard, D. Saltzberg, C. Schnaible, V. Valuev

University of California, Riverside, Riverside, U.S.A.

E. Bouvier, K. Burt, R. Clare, J. Ellison, J.W. Gary, S.M.A. Ghiasi Shirazi, G. Hanson, G. Karapostoli, E. Kennedy, F. Lacroix, O.R. Long, M. Olmedo Negrete, M.I. Paneva, W. Si, L. Wang, H. Wei, S. Wimpenny, B. R. Yates

University of California, San Diego, La Jolla, U.S.A.

J.G. Branson, S. Cittolin, M. Derdzinski, R. Gerosa, D. Gilbert, B. Hashemi, A. Holzner, D. Klein, G. Kole, V. Krutelyov, J. Letts, M. Masciovecchio, D. Olivito, S. Padhi, M. Pieri, M. Sani, V. Sharma, S. Simon, M. Tadel, A. Vartak, S. Wasserbaech[67], J. Wood, F. Würthwein, A. Yagil, G. Zevi Della Porta

University of California, Santa Barbara - Department of Physics, Santa Barbara, U.S.A.

N. Amin, R. Bhandari, J. Bradmiller-Feld, C. Campagnari, M. Citron, A. Dishaw, V. Dutta, M. Franco Sevilla, L. Gouskos, R. Heller, J. Incandela, A. Ovcharova, H. Qu, J. Richman, D. Stuart, I. Suarez, J. Yoo

California Institute of Technology, Pasadena, U.S.A.

D. Anderson, A. Bornheim, J. Bunn, J.M. Lawhorn, H.B. Newman, T. Q. Nguyen, C. Pena, M. Spiropulu, J.R. Vlimant, R. Wilkinson, S. Xie, Z. Zhang, R.Y. Zhu

Carnegie Mellon University, Pittsburgh, U.S.A.

M.B. Andrews, T. Ferguson, T. Mudholkar, M. Paulini, J. Russ, M. Sun, H. Vogel, I. Vorobiev, M. Weinberg

University of Colorado Boulder, Boulder, U.S.A.

J.P. Cumalat, W.T. Ford, F. Jensen, A. Johnson, M. Krohn, S. Leontsinis, E. MacDonald, T. Mulholland, K. Stenson, K.A. Ulmer, S.R. Wagner

Cornell University, Ithaca, U.S.A.

J. Alexander, J. Chaves, Y. Cheng, J. Chu, A. Datta, K. Mcdermott, N. Mirman, J.R. Patterson, D. Quach, A. Rinkevicius, A. Ryd, L. Skinnari, L. Soffi, S.M. Tan, Z. Tao, J. Thom, J. Tucker, P. Wittich, M. Zientek

Fermi National Accelerator Laboratory, Batavia, U.S.A.

S. Abdullin, M. Albrow, M. Alyari, G. Apollinari, A. Apresyan, A. Apyan, S. Banerjee, L.A.T. Bauerdick, A. Beretvas, J. Berryhill, P.C. Bhat, G. Bolla[†], K. Burkett, J.N. Butler, A. Canepa, G.B. Cerati, H.W.K. Cheung, F. Chlebana, M. Cremonesi, J. Duarte, V.D. Elvira, J. Freeman, Z. Gecse, E. Gottschalk, L. Gray, D. Green, S. Grünendahl, O. Gutsche, J. Hanlon, R.M. Harris, S. Hasegawa, J. Hirschauer, Z. Hu, B. Jayatilaka, S. Jindariani, M. Johnson, U. Joshi, B. Klima, M.J. Kortelainen, B. Kreis, S. Lammel, D. Lincoln, R. Lipton, M. Liu, T. Liu, R. Lopes De Sá, J. Lykken, K. Maeshima, N. Magini, J.M. Marraffino, D. Mason, P. McBride, P. Merkel, S. Mrenna, S. Nahn, V. O'Dell, K. Pedro, O. Prokofyev, G. Rakness, L. Ristori, A. Savoy-Navarro[68], B. Schneider, E. Sexton-Kennedy, A. Soha, W.J. Spalding, L. Spiegel, S. Stoynev, J. Strait, N. Strobbe, L. Taylor, S. Tkaczyk, N.V. Tran, L. Uplegger, E.W. Vaandering, C. Vernieri, M. Verzocchi, R. Vidal, M. Wang, H.A. Weber, A. Whitbeck, W. Wu

University of Florida, Gainesville, U.S.A.

D. Acosta, P. Avery, P. Bortignon, D. Bourilkov, A. Brinkerhoff, A. Carnes, M. Carver, D. Curry, R.D. Field, I.K. Furic, S.V. Gleyzer, B.M. Joshi, J. Konigsberg, A. Korytov,

K. Kotov, P. Ma, K. Matchev, H. Mei, G. Mitselmakher, K. Shi, D. Sperka, N. Terentyev, L. Thomas, J. Wang, S. Wang, J. Yelton

Florida International University, Miami, U.S.A.

Y.R. Joshi, S. Linn, P. Markowitz, J.L. Rodriguez

Florida State University, Tallahassee, U.S.A.

A. Ackert, T. Adams, A. Askew, S. Hagopian, V. Hagopian, K.F. Johnson, T. Kolberg, G. Martinez, T. Perry, H. Prosper, A. Saha, A. Santra, V. Sharma, R. Yohay

Florida Institute of Technology, Melbourne, U.S.A.

M.M. Baarmand, V. Bhopatkar, S. Colafranceschi, M. Hohlmann, D. Noonan, T. Roy, F. Yumiceva

University of Illinois at Chicago (UIC), Chicago, U.S.A.

M.R. Adams, L. Apanasevich, D. Berry, R.R. Betts, R. Cavanaugh, X. Chen, S. Dittmer, O. Evdokimov, C.E. Gerber, D.A. Hangal, D.J. Hofman, K. Jung, J. Kamin, I.D. Sandoval Gonzalez, M.B. Tonjes, N. Varelas, H. Wang, Z. Wu, J. Zhang

The University of Iowa, Iowa City, U.S.A.

B. Bilki[69], W. Clarida, K. Dilsiz[70], S. Durgut, R.P. Gandrajula, M. Haytmyradov, V. Khristenko, J.-P. Merlo, H. Mermerkaya[71], A. Mestvirishvili, A. Moeller, J. Nachtman, H. Ogul[72], Y. Onel, F. Ozok[73], A. Penzo, C. Snyder, E. Tiras, J. Wetzel, K. Yi

Johns Hopkins University, Baltimore, U.S.A.

B. Blumenfeld, A. Cocoros, N. Eminizer, D. Fehling, L. Feng, A.V. Gritsan, P. Maksimovic, J. Roskes, U. Sarica, M. Swartz, M. Xiao, C. You

The University of Kansas, Lawrence, U.S.A.

A. Al-bataineh, P. Baringer, A. Bean, S. Boren, J. Bowen, J. Castle, S. Khalil, A. Kropivnitskaya, D. Majumder, W. Mcbrayer, M. Murray, C. Rogan, C. Royon, S. Sanders, E. Schmitz, J.D. Tapia Takaki, Q. Wang

Kansas State University, Manhattan, U.S.A.

A. Ivanov, K. Kaadze, Y. Maravin, A. Modak, A. Mohammadi, L.K. Saini, N. Skhirtladze

Lawrence Livermore National Laboratory, Livermore, U.S.A.

F. Rebassoo, D. Wright

University of Maryland, College Park, U.S.A.

A. Baden, O. Baron, A. Belloni, S.C. Eno, Y. Feng, C. Ferraioli, N.J. Hadley, S. Jabeen, G.Y. Jeng, R.G. Kellogg, J. Kunkle, A.C. Mignerey, F. Ricci-Tam, Y.H. Shin, A. Skuja, S.C. Tonwar

Massachusetts Institute of Technology, Cambridge, U.S.A.

D. Abercrombie, B. Allen, V. Azzolini, R. Barbieri, A. Baty, G. Bauer, R. Bi, S. Brandt, W. Busza, I.A. Cali, M. D'Alfonso, Z. Demiragli, G. Gomez Ceballos, M. Goncharov, P. Harris, D. Hsu, M. Hu, Y. Iiyama, G.M. Innocenti, M. Klute, D. Kovalskyi, Y.-J. Lee, A. Levin, P.D. Luckey, B. Maier, A.C. Marini, C. Mcginn, C. Mironov, S. Narayanan,

X. Niu, C. Paus, C. Roland, G. Roland, G.S.F. Stephans, K. Sumorok, K. Tatar, D. Velicanu, J. Wang, T.W. Wang, B. Wyslouch, S. Zhaozhong

University of Minnesota, Minneapolis, U.S.A.

A.C. Benvenuti, R.M. Chatterjee, A. Evans, P. Hansen, S. Kalafut, Y. Kubota, Z. Lesko, J. Mans, S. Nourbakhsh, N. Ruckstuhl, R. Rusack, J. Turkewitz, M.A. Wadud

University of Mississippi, Oxford, U.S.A.

J.G. Acosta, S. Oliveros

University of Nebraska-Lincoln, Lincoln, U.S.A.

E. Avdeeva, K. Bloom, D.R. Claes, C. Fangmeier, F. Golf, R. Gonzalez Suarez, R. Kamalieddin, I. Kravchenko, J. Monroy, J.E. Siado, G.R. Snow, B. Stieger

State University of New York at Buffalo, Buffalo, U.S.A.

J. Dolen, A. Godshalk, C. Harrington, I. Iashvili, D. Nguyen, A. Parker, S. Rappoccio, B. Roozbahani

Northeastern University, Boston, U.S.A.

G. Alverson, E. Barberis, C. Freer, A. Hortiangtham, A. Massironi, D.M. Morse, T. Orimoto, R. Teixeira De Lima, T. Wamorkar, B. Wang, A. Wisecarver, D. Wood

Northwestern University, Evanston, U.S.A.

S. Bhattacharya, O. Charaf, K.A. Hahn, N. Mucia, N. Odell, M.H. Schmitt, K. Sung, M. Trovato, M. Velasco

University of Notre Dame, Notre Dame, U.S.A.

R. Bucci, N. Dev, M. Hildreth, K. Hurtado Anampa, C. Jessop, D.J. Karmgard, N. Kellams, K. Lannon, W. Li, N. Loukas, N. Marinelli, F. Meng, C. Mueller, Y. Musienko[37], M. Planer, A. Reinsvold, R. Ruchti, P. Siddireddy, G. Smith, S. Taroni, M. Wayne, A. Wightman, M. Wolf, A. Woodard

The Ohio State University, Columbus, U.S.A.

J. Alimena, L. Antonelli, B. Bylsma, L.S. Durkin, S. Flowers, B. Francis, A. Hart, C. Hill, W. Ji, T.Y. Ling, W. Luo, B.L. Winer, H.W. Wulsin

Princeton University, Princeton, U.S.A.

S. Cooperstein, O. Driga, P. Elmer, J. Hardenbrook, P. Hebda, S. Higginbotham, A. Kalogeropoulos, D. Lange, J. Luo, D. Marlow, K. Mei, I. Ojalvo, J. Olsen, C. Palmer, P. Piroué, J. Salfeld-Nebgen, D. Stickland, C. Tully

University of Puerto Rico, Mayaguez, U.S.A.

S. Malik, S. Norberg

Purdue University, West Lafayette, U.S.A.

A. Barker, V.E. Barnes, S. Das, L. Gutay, M. Jones, A.W. Jung, A. Khatiwada, D.H. Miller, N. Neumeister, C.C. Peng, H. Qiu, J.F. Schulte, J. Sun, F. Wang, R. Xiao, W. Xie

Purdue University Northwest, Hammond, U.S.A.

T. Cheng, N. Parashar

Rice University, Houston, U.S.A.

Z. Chen, K.M. Ecklund, S. Freed, F.J.M. Geurts, M. Guilbaud, M. Kilpatrick, W. Li, B. Michlin, B.P. Padley, J. Roberts, J. Rorie, W. Shi, Z. Tu, J. Zabel, A. Zhang

University of Rochester, Rochester, U.S.A.

A. Bodek, P. de Barbaro, R. Demina, Y.t. Duh, T. Ferbel, M. Galanti, A. Garcia-Bellido, J. Han, O. Hindrichs, A. Khukhunaishvili, K.H. Lo, P. Tan, M. Verzetti

The Rockefeller University, New York, U.S.A.

R. Ciesielski, K. Goulianos, C. Mesropian

Rutgers, The State University of New Jersey, Piscataway, U.S.A.

A. Agapitos, J.P. Chou, Y. Gershtein, T.A. Gómez Espinosa, E. Halkiadakis, M. Heindl, E. Hughes, S. Kaplan, R. Kunnawalkam Elayavalli, S. Kyriacou, A. Lath, R. Montalvo, K. Nash, M. Osherson, H. Saka, S. Salur, S. Schnetzer, D. Sheffield, S. Somalwar, R. Stone, S. Thomas, P. Thomassen, M. Walker

University of Tennessee, Knoxville, U.S.A.

A.G. Delannoy, J. Heideman, G. Riley, K. Rose, S. Spanier, K. Thapa

Texas A&M University, College Station, U.S.A.

O. Bouhali[74], A. Castaneda Hernandez[74], A. Celik, M. Dalchenko, M. De Mattia, A. Delgado, S. Dildick, R. Eusebi, J. Gilmore, T. Huang, T. Kamon[75], R. Mueller, Y. Pakhotin, R. Patel, A. Perloff, L. Perniè, D. Rathjens, A. Safonov, A. Tatarinov

Texas Tech University, Lubbock, U.S.A.

N. Akchurin, J. Damgov, F. De Guio, P.R. Dudero, J. Faulkner, E. Gurpinar, S. Kunori, K. Lamichhane, S.W. Lee, T. Mengke, S. Muthumuni, T. Peltola, S. Undleeb, I. Volobouev, Z. Wang

Vanderbilt University, Nashville, U.S.A.

S. Greene, A. Gurrola, R. Janjam, W. Johns, C. Maguire, A. Melo, H. Ni, K. Padeken, J.D. Ruiz Alvarez, P. Sheldon, S. Tuo, J. Velkovska, Q. Xu

University of Virginia, Charlottesville, U.S.A.

M.W. Arenton, P. Barria, B. Cox, R. Hirosky, M. Joyce, A. Ledovskoy, H. Li, C. Neu, T. Sinthuprasith, Y. Wang, E. Wolfe, F. Xia

Wayne State University, Detroit, U.S.A.

R. Harr, P.E. Karchin, N. Poudyal, J. Sturdy, P. Thapa, S. Zaleski

University of Wisconsin - Madison, Madison, WI, U.S.A.

M. Brodski, J. Buchanan, C. Caillol, D. Carlsmith, S. Dasu, L. Dodd, S. Duric, B. Gomber, M. Grothe, M. Herndon, A. Hervé, U. Hussain, P. Klabbers, A. Lanaro, A. Levine, K. Long, R. Loveless, V. Rekovic, T. Ruggles, A. Savin, N. Smith, W.H. Smith, N. Woods

†: Deceased

1: Also at Vienna University of Technology, Vienna, Austria

2: Also at IRFU, CEA, Université Paris-Saclay, Gif-sur-Yvette, France

3: Also at Universidade Estadual de Campinas, Campinas, Brazil

4: Also at Federal University of Rio Grande do Sul, Porto Alegre, Brazil

5: Also at Universidade Federal de Pelotas, Pelotas, Brazil

6: Also at Université Libre de Bruxelles, Bruxelles, Belgium

7: Also at Institute for Theoretical and Experimental Physics, Moscow, Russia

8: Also at Joint Institute for Nuclear Research, Dubna, Russia

9: Also at Helwan University, Cairo, Egypt

10: Now at Zewail City of Science and Technology, Zewail, Egypt

11: Now at Ain Shams University, Cairo, Egypt

12: Also at Department of Physics, King Abdulaziz University, Jeddah, Saudi Arabia

13: Also at Université de Haute Alsace, Mulhouse, France

14: Also at Skobeltsyn Institute of Nuclear Physics, Lomonosov Moscow State University, Moscow, Russia

15: Also at Tbilisi State University, Tbilisi, Georgia

16: Also at CERN, European Organization for Nuclear Research, Geneva, Switzerland

17: Also at RWTH Aachen University, III. Physikalisches Institut A, Aachen, Germany

18: Also at University of Hamburg, Hamburg, Germany

19: Also at Brandenburg University of Technology, Cottbus, Germany

20: Also at MTA-ELTE Lendület CMS Particle and Nuclear Physics Group, Eötvös Loránd University, Budapest, Hungary

21: Also at Institute of Nuclear Research ATOMKI, Debrecen, Hungary

22: Also at Institute of Physics, University of Debrecen, Debrecen, Hungary

23: Also at Indian Institute of Technology Bhubaneswar, Bhubaneswar, India

24: Also at Institute of Physics, Bhubaneswar, India

25: Also at Shoolini University, Solan, India

26: Also at University of Visva-Bharati, Santiniketan, India

27: Also at University of Ruhuna, Matara, Sri Lanka

28: Also at Isfahan University of Technology, Isfahan, Iran

29: Also at Yazd University, Yazd, Iran

30: Also at Plasma Physics Research Center, Science and Research Branch, Islamic Azad University, Tehran, Iran

31: Also at Università degli Studi di Siena, Siena, Italy

32: Also at INFN Sezione di Milano-Bicocca; Università di Milano-Bicocca, Milano, Italy

33: Also at International Islamic University of Malaysia, Kuala Lumpur, Malaysia

34: Also at Malaysian Nuclear Agency, MOSTI, Kajang, Malaysia

35: Also at Consejo Nacional de Ciencia y Tecnología, Mexico city, Mexico

36: Also at Warsaw University of Technology, Institute of Electronic Systems, Warsaw, Poland

37: Also at Institute for Nuclear Research, Moscow, Russia

38: Now at National Research Nuclear University 'Moscow Engineering Physics Institute' (MEPhI), Moscow, Russia

39: Also at St. Petersburg State Polytechnical University, St. Petersburg, Russia

40: Also at University of Florida, Gainesville, U.S.A.

41: Also at P.N. Lebedev Physical Institute, Moscow, Russia

42: Also at California Institute of Technology, Pasadena, U.S.A.

43: Also at Budker Institute of Nuclear Physics, Novosibirsk, Russia

44: Also at Faculty of Physics, University of Belgrade, Belgrade, Serbia

45: Also at INFN Sezione di Pavia; Università di Pavia, Pavia, Italy

46: Also at University of Belgrade, Faculty of Physics and Vinca Institute of Nuclear Sciences, Belgrade, Serbia

47: Also at Scuola Normale e Sezione dell'INFN, Pisa, Italy

48: Also at National and Kapodistrian University of Athens, Athens, Greece

49: Also at Riga Technical University, Riga, Latvia

50: Also at Universität Zürich, Zurich, Switzerland

51: Also at Stefan Meyer Institute for Subatomic Physics (SMI), Vienna, Austria

52: Also at Adiyaman University, Adiyaman, Turkey

53: Also at Istanbul Aydin University, Istanbul, Turkey

54: Also at Mersin University, Mersin, Turkey

55: Also at Piri Reis University, Istanbul, Turkey

56: Also at Gaziosmanpasa University, Tokat, Turkey

57: Also at Izmir Institute of Technology, Izmir, Turkey

58: Also at Necmettin Erbakan University, Konya, Turkey

59: Also at Marmara University, Istanbul, Turkey

60: Also at Kafkas University, Kars, Turkey

61: Also at Istanbul Bilgi University, Istanbul, Turkey

62: Also at Rutherford Appleton Laboratory, Didcot, United Kingdom

63: Also at School of Physics and Astronomy, University of Southampton, Southampton, United Kingdom

64: Also at Monash University, Faculty of Science, Clayton, Australia

65: Also at Instituto de Astrofísica de Canarias, La Laguna, Spain

66: Also at Bethel University, ST. PAUL, U.S.A.

67: Also at Utah Valley University, Orem, U.S.A.

68: Also at Purdue University, West Lafayette, U.S.A.

69: Also at Beykent University, Istanbul, Turkey

70: Also at Bingol University, Bingol, Turkey

71: Also at Erzincan University, Erzincan, Turkey

72: Also at Sinop University, Sinop, Turkey

73: Also at Mimar Sinan University, Istanbul, Istanbul, Turkey

74: Also at Texas A&M University at Qatar, Doha, Qatar

75: Also at Kyungpook National University, Daegu, Korea